Constraining the large scale glaciation of Antarctica during the Eocene-Oligocene Transition using hydrogen isotopes of alkenones

Andrew J P Ward

(4101375)

In part fulfilment of the requirements for the degree of

Master of Science in Earth Science at Utrecht University

13 September 2015

Supervised by:

Prof. Dr. Stefan Schouten (UU, NIOZ) & Dr. Marcel van der Meer (NIOZ)

Universiteit Utrecht

Koninklijk Nederlands Instituut
voor Onderzoek der Zee
Marine Organic Biogeochemistry
Department

Statement of originality of the MSc thesis

I declare that:

1. This is an original report, which is entirely my own work,

2. Where I have made use of the ideas of other writers, I have acknowledged the source in all instances,

3. Where I have used any diagram or visuals I have acknowledged the source in all instances,

4. This report has not and will not be submitted elsewhere for academic assessment in any other academic course.

Name: Andrew Ward

Registration number: 4101375

Date: 13/09/2015

Abstract

The Eocene/Oligocene Transition (EOT) (34 Ma) represents a fundamental moment in the history of the Earth. A 1.5‰ positive oxygen isotope excursion marks the transition from an Earth that was warm and largely ice-free towards one of significant glacial ice and cooler temperatures, which still resides today. The EOT is also associated with the origination of the Antarctic Ice Sheet (AIS), however despite much study the cause of this momentous episode of ice growth is widely disputed. Here, the hydrogen isotopes of C37 alkenones are used to reconstruct ice growth over the EOT from three Atlantic sediment cores. The results presented here show a strong positive ~20‰ hydrogen isotope excursion occurring with the EOT suggesting significant Antarctic ice growth. More significantly though, this hydrogen isotope excursion occurs prior to the major oxygen isotope excursion suggesting glaciation prior to abyssal temperature decrease. This is supported by a $U_{37}^{K'}$ SST reconstruction showing major cooling of ~5^{o}C occurring after the hydrogen isotope shift. This trend of ice growth first and subsequent abyssal cooling suggests atmospheric carbon dioxide drawdown as the cause for the origin of Antarctic glaciation.

Acknowledgements

I would like to thank Marcel van der Meer not only for his continued guidance and advice throughout the research and writing phases of this project at NIOZ but also for providing me with the data from site 511 which has increased the value of this thesis greatly. I would also like to thank Stefan Schouten for offering me the opportunity to come and complete the research for this thesis at the NIOZ on Texel. The experience and knowledge I have gained during this period is worth many times more than simply the writing of this thesis.

I would also like to take this opportunity as the culmination of my two-year masters degree in the Netherlands to thank someone who will never read this thesis but without whom I could not have written it; Kirstie Hubbard for her support and patience throughout these long two years away.

Contents

1. Introduction

i. The Eocene/Oligocene (E/O) boundary

The Eocene/Oligocene (E/O) boundary is recognised as the most significant extinction event of the Cenozoic, effecting the flora and fauna of both marine (Ivany et al., 2000; Pearson et al., 2008) and terrestrial (Keller et al., 1992; Hooker et al., 2004) ecosystems. The formal definition of the E/O boundary at 33.7 Ma is the last occurrence (LO) of the planktonic foraminifera family *Hantkeninideae* at the Umbria-Marche Basin, Italy (Pearson et al., 2008).

This mass extinction event coincides with a significantly increased presence of ice on Antarctica. A drop in the carbon compensation depth (CCD) and pronounced hiatuses in sedimentary sections at shallow marine sites provide circumstantial evidence for continental shelf exposure and therefore sea level fall (Stickley et al., 2004; Coxall et al., 2005). Quantitative sea level estimates based on sedimentology and biotic analysis find a global sea level fall of between 70-100m (Miller et al., 2009; Houben et al., 2012; Wade et al., 2012). Global scale sea level change on this scale must have been caused by continental ice growth (Miller et al., 2009).

In addition, ice rafted debris (IRD) is found in Southern Ocean drill cores from approximately 34 Ma onwards (Zachos et al., 1992; Zachos et al., 1996; Ivany et al., 2006) suggesting glacial ice extending to sea level; with studies of clay mineralogy (Robert & Kennett, 1997; Ehrmann, W., 1998), magnetite deposition (Sagnotti et al., 2001) and terrestrial palynology (Francis et al., 2008) showing a corresponding increased ice influence on the Antarctic continental interior (Ehrmann et al., 1992).

The compelling evidence for a rapid sea level drop combined with ice volume and temperature reconstructions suggests a substantial Antarctic glaciation originating across the E/O boundary. The Antarctic continent was transformed from holding only very small, isolated glaciers to being fully glaciated, with an ice sheet approximately 55 - 125% the size of the present-day Antarctic ice sheet (AIS) (Katz et al., 2008) in only 300kyr (Coxall et al., 2005).

ii. The Eocene/Oligocene Transition

The initial large-scale glaciation of Antarctica at the Eocene/Oligocene boundary represents a fundamental moment in the climate history of the Earth. For a long period before this time the Earth's atmosphere was likely rich in CO_2 and the Earth's surface warm and largely ice free (Pagani et al., 2002). Straddling the E/O boundary a sharp 1.5‰ positive oxygen isotope excursion, recorded in the $\delta^{18}O$ of benthic foraminifera tests ($\delta^{18}O_b$), marks the beginning of a glaciated world with global temperatures and atmospheric CO_2 generally decreasing ever since (Zachos et al., 1996).

The Eocene/Oligocene Transition (EOT) is the ~500kyr climate transition that encompasses this entire oxygen isotope excursion across the E/O boundary, from 33.9-33.4Ma (Coxall & pearson, 2007). In high resolution records the excursion can be seen to occur in two distinct steps, both with 40kyr durations and separated by a 200kyr plateau (Coxall et al., 2005). The timing and relative contribution of these steps to the overall 1.5‰ $\delta^{18}O$ shift differs slightly between studies (Coxall et al., 2005; Miller et al., 2008; Miller et al., 2009; Houben et al., 2012), however most settle on the first of these steps, termed EOT event 1 (EOT-1), occurring at ~33.8Ma with the second step, termed the Oligocene isotope event 1 (Oi-1), occurring at ~33.5Ma (Katz et al., 2008) with relative contributions of ~0.5‰ and ~1‰ respectively (Pusz et al., 2011).

The $\delta^{18}O$ of seawater ($\delta^{18}O_w$) varies through time due to a variety of processes. The primary factor on large timescales is the 'ice volume effect' which relates to the waxing and waning of global ice sheets (Shackleton, 1967). Due to fractionation associated with Rayleigh distillation, ice at the poles is enriched in ^{16}O relative to ^{18}O (Rohling & Cooke, 2003). The consequence of this is the preferential removal of ^{16}O from the sea water with increase glacial ice growth, which therefore increases the $\delta^{18}O_w$.

The $\delta^{18}O_w$ is reflected in the oxygen within the carbonate (CO_3^{2-}) dissolved in the sea water. Many foraminifera species build calcium carbonate ($CaCO_3$) tests, constructed from this carbonate along with calcium ions (Ca^+) which are also dissolved in the surrounding water. As a result the $\delta^{18}O_w$ is

reflected in the foraminifera tests (Spero et al., 1997). However, in addition to purely reflecting the $\delta^{18}O_w$, there is a temperature dependent oxygen isotope fractionation by the foraminifera during calcification (Urey, 1947). That is, at increased temperatures, relatively more ^{16}O is incorporated into the foraminifera tests (Ravelo & Hillaire-Marcel, 2007). The overall outcome of this is that the $\delta^{18}O_b$ record includes both an ice volume and a temperature component.

Traditional thinking holds that these two $\delta^{18}O_b$ components are separately related to the two $\delta^{18}O$ steps, EOT-1 and Oi-1. Following this line of thinking the first step, EOT-1, is predominantly a temperature signal, i.e. a decrease in bottom water temperature (Katz et al., 2008; Lear et al., 2008; Miller et al., 2008), whereas Oi-1 is predominantly ice volume driven, i.e. an increase in Antarctic ice volume (Zachos et al., 1996; Coxall et al., 2005; Katz et al., 2008; Miller et al., 2009). In this traditional idea, first there was abyssal water cooling and this was then followed by ice growth, with CO_2 reduction being a secondary effect of the cooling (Livermore et al., 2007). This last point is however beginning to be questioned (Goldner et al., 2014).

iii. Cause of the original Antarctic glaciation

There are a number of hypothesis being discussed in contemporary literature concerning the cause(s) of Antarctic glaciation.

a) Orbital

The stepwise nature of the $\delta^{18}O$ shift, with its 40 and 200kyr periodicities implies a degree of orbital dependence within the EOT glaciation (Diester-Haass & Zahn, 1996), and indeed this period of earth history experiences significant orbital forcing in both the $\delta^{18}O$ and $\delta^{13}C$ records (Pälike et al., 2006). However the orbital configuration cannot be the sole cause as obliquity and eccentricity nodes which occurred at the EOT were not any more extreme than those that had occurred for at least the previous 40myr (Coxall et al., 2005).

b) Gateway Hypothesis

Plate tectonics caused the Southern Ocean paleogeography to change between the Eocene and Oligocene, with the opening of the Southern Ocean gateways; the Drake Passage (DP) and the Tasman Gateway (TG). Many studies have attempted to establish a timeframe of these openings, with the majority finding these gateways opening at the latest Eocene (Reguero et al., 2002; Diekmann et al., 2004; Stickley et al., 2004; Scher & Martin, 2006; Via & Thomas, 2006; Livermore et al., 2007; Eagles & Jokat, 2014). The co-occurrence of the gateway openings with the origination of Antarctic glaciation has led many to hypothesise a causal link between these openings and Antarctic ice origination, the "gateway hypothesis". The hypothesis follows that these openings allowed the development of the Antarctic Circumpolar Current (ACC), which deflected warm water currents from the north, thermally isolating the Antarctic continent (Kennett, 1977; Diester-Haass & Zahn, 1996; Lawver & Gahagan, 1998; Martos et al., 2013).

This thermal isolation mechanism relies on the presence of warm southward flowing currents reaching the high latitudes throughout the Eocene that were then impeded by the proto-ACC at the EOT (Exon et al., 2002). The effect that these currents had is debated with some models showing that they warmed the polar region, thus keeping it ice free (Sijp et al., 2009; Tigchelaar et al., 2010; Sijp et al., 2011), whilst others show that these warm currents did not reach the high latitudes, and therefore could not have warmed the Antarctic continent (Huber et al., 2004; Huber & Nof et al., 2006). Additional uncertainties are produced through studies that find evidence for either an earlier, Eocene gateway opening (Scher & Martin, 2006), or later Oligocene (Lawver et al., 2003; Geletti et al., 2005; Lodolo et al., 2010) and even Miocene openings (Barker, 2001).

c) Carbon dioxide drawdown hypothesis

Synchronous carbon cycle changes are well documented in the proxy record at numerous sites over the EOT (Coxall et al., 2005; Pagani et al., 2011). A large 1‰ excursion in benthic foraminifera $\delta^{13}C$ ($\delta^{13}C_b$) (Coxall et al., 2005; Tigchelaar et al., 2010) and a 1km deepening of the carbon compensation

depth (CCD) (Coxall et al., 2005) both co-occur with the $\delta^{18}O_b$ shift. Both of these events are strongly linked to atmospheric CO_2 concentration (pCO_2) decline (Coxall et al., 2005; Tigchelaar et al., 2010).

The carbon drawdown hypothesis was developed based on this early evidence for a large carbon cycle perturbation (Anderson & Delaney, 2005; Zachos & Klump, 2005; Goldner et al., 2014). This hypothesis holds that pCO_2 fell below a threshold which allowed temperatures low enough, during orbital nodes, to force small Antarctic glaciations (Coxall et al., 2005). Below this threshold, these small glaciations triggered positive feedbacks including; albedo (Pollard & DeConto, 2005), height-mass balance - whereby increases in ice sheet height and mass create conditions for reduced ablation (Ladant et al., 2014), and continental shelf exposure (Goldner et al., 2014), resulting in rapid continental ice growth (DeConto & Pollard, 2003).

$\delta^{13}C_b$ has been used to estimate a 2-5 fold pCO_2 decrease across the EOT (Anderson & Delaney, 2005) with the $\delta^{13}C$ of alkenones ($\delta^{13}C_{alk}$) showing a ~40% reduction in pCO_2 across the EOT over multiple sites (Pagani et al., 2011) whilst boron isotopes within foraminifera tests ($\delta^{11}B_{carbonate}$) have estimated that pCO_2 fell below ~750ppm during the maximum ice growth at the EOT (Pearson et al., 2009).

$\delta^{13}C_b$ has been used to estimate a 2-5 fold pCO_2 decrease across the EOT (Anderson & Delaney, 2005) with the $\delta^{13}C$ of alkenones ($\delta^{13}C_{alk}$) showing a ~40% pCO_2 reduction (Pagani et al., 2011), whilst boron isotopes within foraminifera tests ($\delta^{11}B_{carbonate}$) have estimated that pCO_2 fell below ~750ppm during the maximum ice growth at the EOT (Pearson et al., 2009).

There is broad agreement between most modelled threshold estimates of 700-900ppm (DeConto & Pollard, 2003; Pearson et al., 2009; Ladant et al., 2014), which roughly equal the estimates from pCO_2 proxies over the EOT and therefore offers strong evidence for the CO_2 hypothesis (Ladant et al., 2014). However this relatively high threshold limit is not agreed on by all studies, with some models finding much lower threshold limits, which are too low to have been crossed during the EOT (Tigchelaar et al., 2010).

The large uncertainties relating to the pCO_2 proxies, with $\delta^{13}C_{alk}$ depending much more heavily on growth rate than on pCO_2 (Benthien et al., 2002) and $\delta^{11}B_{carbonate}$ showing strong temperature and salinity dependence (Pagani et al., 2005; Hemming & Hönisch, 2007), lead many to question their estimates (Pagani et al., 2005; Livermore et al., 2007). It has been suggested that the drop in CCD could have resulted from sea level fall caused by ice volume increase rather than decreased CO_2 (Livermore et al., 2007). Moreover, data from sea temperature proxies do not fit with a CO_2 drawdown as sea surface temperature (SST) cooling rates are larger at high southern latitudes than equatorial or northern latitudes (Lear et al., 2008; Liu et al., 2009). This provides evidence against widespread CO_2 drawdown, as this drawdown should be globally uniform and therefore approximately cool SSTs equally (Goldner et al., 2014). Also studies argue that CO_2 drawdown could not have caused the deep sea cooling seen at the EOT, or indeed the circulation change and ocean stratification seen in proxies (Katz et al., 2011; Goldner et al., 2014).

d) Antarctic ice feedback hypothesis

A more recently emerging hypothesis is an advancement of the CO_2 drawdown hypothesis; however it better describes the oceanographic changes seen in proxies. Following the CO_2 drawdown hypothesis, this 4th hypothesis holds that CO_2 drawdown below a threshold allowed a small glaciation. This newly glaciated continent led to increased sea ice growth and thus brine rejection, leading to sinking around the continental margins and the subsequent formation of Antarctic bottom water (Miller et al., 2009) and proto-ACC (Hogg et al., 2010; Goldner et al., 2014; Ladant et al., 2014), as well as the strengthening of Antarctic intermediate water (AIW) (Goldner et al., 2014). The glaciation also led to increased wind-driven currents around the Antarctic margin leading to increased mixing and productivity (Goldner et al., 2014; Ladant et al., 2014). It is therefore feedbacks relating to the onset of glaciation itself, caused by CO_2 drawdown, which are seen in proxies (Miller et al., 2009; Goldner et al., 2014).

iv. Decoupling ice and temperature from $\delta^{18}O$

The gateway hypothesis relies on abyssal cooling around Antarctica caused by a reduction in warm currents, followed by glaciation. Conversely CO_2 drawdown, with AIS feedbacks, rejects this conventional view and instead suggests glaciation occurred first, which then caused the abyssal cooling through the feedbacks previously discussed.

By constraining the relative timings of ice growth and temperature decrease across the EOT it may be possible to provide evidence in favour of either hypothesis (Lear et al., 2004; Liu et al., 2009). In order to do this many studies attempt to detangle these components from the $\delta^{18}O$ record by independently reconstructing one in order to remove this from the overall $\delta^{18}O$, and therefore isolate the effect of the other.

a) Temperature

Using the Mg/Ca temperature proxy on foraminifera from cores from deep-sea sites with exceptional preservation, well above the CCD, studies show a ~2.5^{o}C benthic cooling occurring at EOT-1, with little cooling occurring at Oi-1 (Katz et al., 2008; Lear et al., 2008). This cooling at the EOT-1 translates to a ~0.5‰ $\delta^{18}O$ change and so suggests that the entire 0.5‰ EOT-1 step is attributed to cooling alone, and correspondingly, the lack of cooling at Oi-1 suggests this step is attributed to ice growth (Lear et al., 2008). This cooling then ice growth trend across the EOT is supported by major turnovers in temperature sensitive dinoflagellates which occur at EOT-1, but not at Oi-1 (Wade et al., 2012).

Other studies have attempted to use organic temperature proxies such as $U_{37}^{K'}$ and TEX_{86} to validate these findings (Liu et al., 2009). They estimate a 3-5^{o}C benthic cooling across the EOT; however such reconstructions are derived from other organisms than foraminifera, dwelling in the surface ocean. This means that a coupled atmosphere-ocean model is required to translate these SST estimates to benthic values, introducing additional uncertainties. Furthermore the difference in the source organisms mean that they may yield different temperature estimates than the Mg/Ca temperatures and therefore complicates their comparison.

b) Ice volume

Eustatic sea level change is largely forced by changes in continental ice volume. As a result some studies have attempted to use sea level changes at the EOT to reconstruct ice volume and therefore untangle the $\delta^{18}O$ signal.

Sea level reconstructions mostly agree on a relatively minor sea level fall occurring at EOT-1 of 20m (Miller at al., 2009; Houben et al., 2012; Wade et al., 2012), with Miller et al. (2008) finding no sea level change at all occurring with this first isotope step. The estimates for Oi-1 sea level change are much higher, ranging from 50m to 80m (Miller at al., 2008; Katz et al., 2008; Miller at al., 2009; Houben et al., 2012; Wade et al., 2012). Using these sea level estimates studies then estimate the ice volume change occurring at both $\delta^{18}O$ steps. Similarly to those studies in the previous section, there is agreement that the first step, EOT-1, is mostly related to temperature whereas major ice growth occurs at Oi-1.

This trend of abyssal cooling first, then ice growth across the EOT lends support to the gateway hypothesis rather than the CO_2 drawdown hypothesis. However both of the methods above have significant flaws. Firstly for both methods suitable core sites are scarce because of Mg/Ca preservation issues (Lear et al., 2008) and localised tectonic changes (Kominz et al., 2008) meaning the number of studies, as well as their global distribution, are very limited. The sea level estimates are effected by localised sea level change, which is effected by tectonic changes (Kominz et al., 2008), ocean circulation (Stocchi et al., 2013) and proximity to ice growth (Wade et al., 2012).

v. Hydrogen isotopes of alkenones

Similarly to oxygen isotopes, the hydrogen isotopes of water (^1H & D) also experience fractionation associated with Rayleigh distillation. Again it is water containing the lighter isotope (^1H) that is preferentially incorporated into ice sheets, leaving the heavier isotope (D) relatively more abundant in the remaining sea water (Gat & Gonfiantini, 1981). This tight coupling between oxygen and hydrogen isotopes is shown in the meteoric water line, in which $\delta D = 8 \times \delta^{18}O + 10‰$ (Craig, 1961).

Due to the difficulties in untangling the separate ice and temperature components of the foraminifera $\delta^{18}O$ record this study attempts instead to focus on hydrogen isotopes.

The hydrogen isotopic composition of sea water (δD_w) is reflected in the hydrogen isotopes of organic matter. Unfortunately bulk organic matter contains substantial amounts of exchangeable hydrogen and therefore loses its original δD signature; however lipids produced by marine organisms contain much less exchangeable hydrogen and therefore somewhat avoid this problem.

Long-chained, unsaturated ethyl and methyl ketones (alkenones) are produced primarily by a select group of haptophyte algae (Brassell et al., 2014). The most prominent of these algae in the modern ocean, *Emiliania huxleyi* and *Gephyrocapsa oceanica,* extend only as far back as the late Pleistocene and early Pliocene respectively (Pagani et al., 2002), however in a review by Brassell (2014) and references therein, on the Paleogene evolution of alkenones the authors show that alkenone producers across the Paleogene originate from three genera within the family Noelaerhabdaceae which have a direct lineage to the modern-day producers, suggesting a similar alkenone biosynthesis pathway and therefore similar fractionation (Pagani et al. 2002). Due to the widespread usage of $U_{37}^{K'}$ (Brassell et al., 1986) and $\delta^{13}C_{alk}$ for CO_2 proxies, alkenones have been well studied in both cultures and sediments. More recently the δD of alkenones (δD_{alk}) has been particularly well studied due to its application as a salinity proxy (van der Meer et al., 2007; van der Meer et al., 2008).

Unlike many other organic compounds (e.g. sterols), alkenones contain only non-exchangable hydrogen. As this hydrogen is not readily interchanged the alkenone δD should largely reflect its original δD composition (Sessions et al., 1999). Concentrating on one molecular species, namely C_{37} alkenones, removes the problems of preferential preservation and organic matter origin that are related to the analysis of bulk lipids (Andersen et al., 2001; Wolhowe et al., 2009).

As with all organic lipids, the alkenones reflect the δD_w in which they were produced. In addition to this, fractionation occurs between the sea water and the alkenones during biosynthesis (δD_w- δD_{alk}).

Schouten et al. (2006) found that this fractionation depends on the salinity and growth rate, but not temperature.

Continental ice has a very low salinity and is highly depleted in δD. This leads to an increase in sea water salinity and δD_w enrichment with increased glaciation. As both increased δD_w and salinity create an increased δD_{alk} (Schouten et al., 2006) the salinity effect on alkenone fractionation could amplify the ice signal; however localised salinity changes could complicate the simple δD_w-δD_{alk} relationship (Wolhowe et al., 2009). The growth phase effect appears as a reduction in fractionation, thus reduced deuterium incorporation, with increased growth rate. As no reliable proxy yet exists for growth rate, the growth phase effect cannot be accommodated for (Wolhowe et al., 2009). However, together with other biological effects such as differences in light intensities (van der Meer et al., 2015) and species composition (M'Boule et al., 2014) which have also been shown to affect the simple δD_w-δD_{alk} fractionation the growth rate can largely be ignored. This is because these are integrated over the large timescales that are handled by this study, with many different light intensities, growth rates and species compositions being experienced over the thousands of years between samples and therefore their effects average out.

Further fractionation differences occur between degrees of alkenone unsaturation (Wolhowe et al., 2009). This is that the tri-unsaturated alkenone species ($C_{37:3}$) is significantly depleted in δD relative to its di-unsaturated counterpart ($C_{37:2}$). Temperature dependant changes in the ratio between the two unsaturation levels (i.e. $U_{37}^{K'}$) then lead to slight temperature dependence in the δD measurement of each alkenone species. To overcome this, van der Meer et al. (2013) suggest measuring the δD of the combined $C_{37:3\&2}$ peaks and determining the δD of C_{37} alkenones which represents the original water isotope value more than the individual alkenones that reflect additional biosynthetic (desaturation) effects.

The lack of temperature dependence and the negligible long-term growth effect means that the δD_{alk} predominantly reflects the δD_w and salinity which in turn both reflect ice volume offering a potential

proxy for ice volume change through time. Through this proxy an increase in δD_{alk} corresponds to an increase in ice volume. Through comparing this signature of ice volume with the $\delta^{18}O_b$ record the separate $\delta^{18}O_b$ components can be decoupled. The use of alkenones will also allow me to reconstruct SST through $U_{37}^{K'}$, providing separate estimates for both of the $\delta^{18}O_b$ components, based on the same compound.

vi. Research questions

This study addresses the research question; *at which $\delta^{18}O$ step of the EOT does the δD_{alk} excursion occur and how does this compare to temperature change?*

This question can be answered through comparison between the δD_{alk} record and SST estimates from $U_{37}^{K'}$ and Tex_{86} produced by this and other studies; with the timings of each $\delta^{18}O_b$ step found through the $\delta^{18}O$ records produced by other studies. The answer to this question will then offer insight into the mechanism of the original glaciation. If the glaciation occurred at the first step (EOT-1) only, this would provide evidence for the CO_2 drawdown hypothesis as the second $\delta^{18}O$ step must be related to abyssal cooling. Equally if the glaciation occurred at the second step (Oi-1) only, this would infer that the first step was temperature related and therefore that abyssal cooling occurred prior to ice growth lending support to the gateway hypothesis. Finally, if there is no excursion observed at all then factors such as local salinity and haptophyte growth rates must be considered.

In order to answer this question several well-dated cores known to contain alkenones across the EOT were analysed to obtain δD_{alk}, $U_{37}^{K'}$ and Tex_{86} values through this transition.

vii. Motivation

The original glaciation of Antarctic at the E/O boundary represents the largest climate transition of the past 65 million years. The fact that the cause of this fundamental transition is still unknown indicates a major gap in the scientific knowledge of the past climate.

In addition, the role of CO_2 over the transition makes it also highly relevant to the study of future climate, as the EOT was the first time since the Permian (Ekart et al., 1999; Berner, 2006) pCO_2 levels fall to values approximating those predicted by the latest IPCC reports (AR5) for the next 100 years (IPCC, 2013). This period can then be used as analogous in climate models for future climate. Furthermore, reconstructing how the AIS originated, as well as understanding the many feedbacks likely associated with it, leads to better predictions of how the ice sheet may change in the future.

The implications of this study then go further in testing whether this δD_{alk} method provides a possible proxy for ice volume to be used to reconstruct other major ice volume changes, such as the Oligocene/Miocene glaciations at ~23 Ma (Mawbey & Lear, 2013) and the northern hemisphere glaciation at ~2.4 Ma (Raymo, 1994).

2. Materials and methods

i. Cores

a) OPD leg 177 site 1090 (42°54.8′S, 8°53.9′E)

This core site is located on the Agulhas Ridge in the sub-Antarctic South Atlantic (figure 1). The recovered core 1090B was drilled to a depth of 397.5mbsf, extending from the late Pleistocene to the middle Eocene. This core has been well dated by Channell et al. (2003) through magneto-, bio-, and chemo-stratigraphy providing sound dating for the core samples received for the purposes of this study. For the uppermost portion of the core, above 221mbsf, the match to the geomagnetic polarity timescale (GPTS) is unequivocal (Scher & Martin, 2008). Two GPTS matches were possible for the remainder of the core and so this part of the core was matched with the aid of Sr, C and O isotopes (Channell et al., 2003).

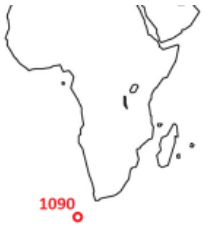

Figure 1. Site 1090: map showing location of ODP site 1090

A total of 19, 25cm^3 core samples were received from the IODP Bremen core repository. These samples range from approximately 150 to 336 mbsf covering the Late Eocene to Late Oligocene. Sample resolution increases significantly around the EOT at depths ~225-250 mbsf, achieving a 3m (~80ky) resolution across the crucial 8 samples which shoulder this transition. Liu et al. (2009) and Pagani et al. (2011) both report alkenones present in this core across the EOT making it an attractive core site for the purposes of this study.

b) OPD leg 151 site 913 (75°29.356'N, 6°56.810'E)

This core site is located in the Greenland Sea, between Greenland and Svalbard (figure 2). The recovered core 913B was drilled to a depth of 684.3mbsf, from the Quaternary through to the middle Eocene. According to Eldrett et al. (2004) core 913B is the best preserved record of Eocene and Oligocene sediments in the high northern latitudes. This preservation has allowed the construction of a highly reliable dating record through the use of magnetostratigraphy

Figure 2. Site 913: map showing location of ODP site 913

and dinoflagellate biostratigraphy by Eldrett et al. (2004). This good preservation also offers encouragement for the presence of alkenones and indeed Liu et al. (2009) have recovered alkenones from this core through a $U_{37}^{K'}$ record spanning the EOT.

A total of 23, 25cm^3 samples were received from the IODP repository. These samples span approximately 140m of the core, from 375 to 516 mbsf, covering the middle Eocene to early Miocene. A sample frequency of ~5m provides a 600kyr resolution throughout the ~20myr span.

c) OPD leg 154 site 925 (4°12.248'N, 43°29.349'W)

This core site is located on the Ceara Rise, off the north-east coast of Brazil, in the equatorial Atlantic Ocean (figure 3). The recovered core 925A was drilled to a depth of 930.4mbsf, extending from the late Pleistocene to middle Eocene (Shipboard Scientific Party, 1995). Due to the lack of extensive hiatuses across the site 925 Chaisson & Pearson (1997) and Pearson & Chaisson (1997) were able to construct a complete age model through the use of planktonic foraminifera biostratigraphy and astrochronology. The core was chosen due to the reported presence of alkenones across the entire middle Eocene to late Oligocene (Pagani et al., 2011; Zhang et al., 2013).

Figure 3. Site 913: map showing location of ODP site 925

From core 925 a total of 28, 25cm^3 core samples were received from the IODP repository. The 28 samples extend over a 130m range, from ~690 to ~820mbsf, covering the Late Eocene to Late Oligocene and achieving a 5m (~150kyr) resolution across the EOT.

ii. Method

a) Alkenone extraction

Each sample was freeze-dried before being crushed into a fine powder using an automated rock mill. Approximately 10-20g of each powdered sample was taken and mixed with diatomaceous earth before being loaded into 33ml metal cells for extraction using an Accelerated Solvent Extractor (ASE; Dionex ASE 350) with dichloromethane:methanol (9:1 v:v) at elevated temperature and pressure (100^{o}C, 1000psi) in three, 5-minute cycles. The total lipid extract (TLE) was subsequently dried in a

40°C water bath under a nitrogen stream using a Turbovap. The dried extract was separated through column chromatography with Al_2O_3 as the stationary phase into an apolar, ketone, and polar fraction using hexane:dichloromethane (9:1, v:v), hexane:dichloromethane (1:1, v:v), and methanol:dichloromethane (1:1, v:v) respectively. Each fraction was collected in a pre-weighed vial and solvents were evaporated under a nitrogen stream leaving a dry extract which could then be weighed.

b) Alkenone identification

The ketone fraction was analysed for long chain alkenones through gas chromatography using a Hewlett Packard 6890 Gas Chromatograph (GC) installed with a 25m CP Sil 5 column 0.32 mm diameter and 0.12 µm film thickness. The ketone fraction was dissolved in ethyl acetate (EtOAc) at a concentration of approximately 1mg/ml, 1µl of this dissolved ketone fraction was injected into the GC. Each sample was introduced to column at 70°C and followed identical 70 minute temperature programs in which temperature was increased by 20°C/min until 130°C, and then by 4°C/min until 320°C, at which point the temperature was held for 20 minutes.

The alkenones within the sample were identified based on their retention time by comparison with an alkenone fraction obtained from an *Emiliania huxleyi* culture that was analyzed on the same GC at the time the samples were analysed (figure 4). These *E. huxleyi* alkenones were identified by gas chromatography-mass spectrometry (GC-MS). Once the compounds within each sample had been identified as alkenones, the maximum amplitude of the C_{37} alkenones was recorded. Samples containing enough alkenones based on peak height and injection volume relative to total volume were deemed to contain sufficient alkenones for reliable δD values. Additional sample material was extracted and separated for those samples that contained significant, but not enough amount of alkenones in an attempt to obtain enough alkenones for reliable δD measurements.

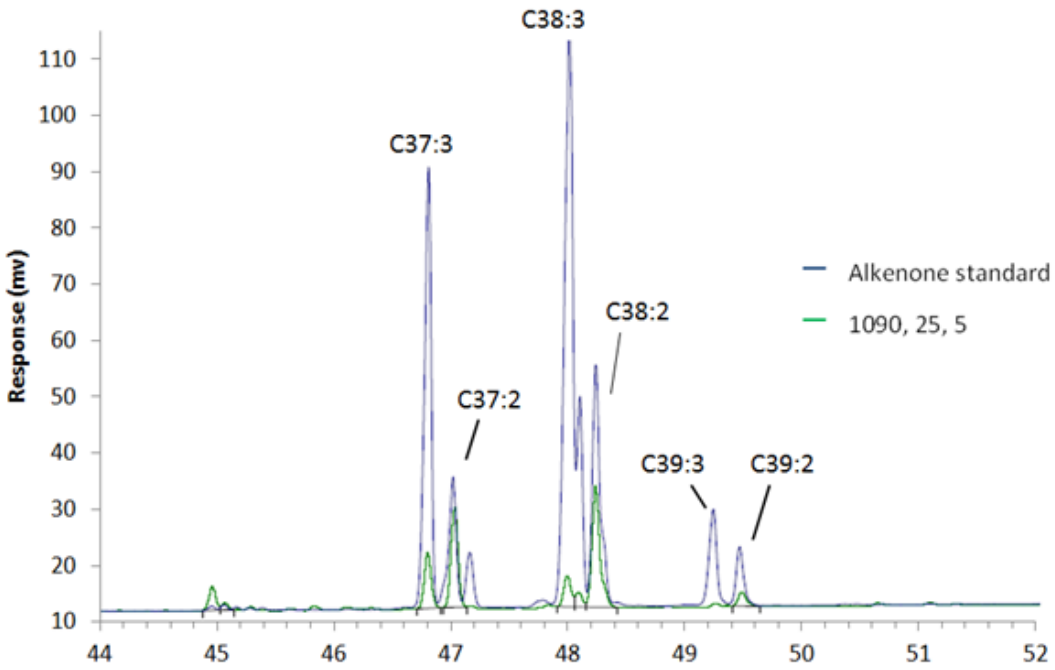

Figure 4. Alkenone identification: The relevant section of the gas chromatograph for the alkenone identification, with the alkenone 'standard' used for alkenone identification plotted against a potential alkenone trace from a sample from site 1090. Alkenone peaks assigned from GC-MS of alkenone standard.

c) Isotopic analysis

Isotopic analysis was performed on ketone fractions containing sufficient C_{37} alkenones. The δD_{alk} was measured on an isotope ratio mass spectrometry (IRMS) with an Agilent 7890A GC connected through a Thermoscientific GC Isolink and Conflo 4 to a Thermoscientific Delta V advantage IRMS. The GC was equipped with a 100% dimethylpolysiloxane coated fused-silica capillary column (Agilent CP-Sil 5 CB; 25m × 0.32 mm ID; film thickness = 0.4 µm). A constant flow of the Helium carrier gas was used at 1 ml/min.

Samples were injected on-column at 70 °C, and the temperature was increased to 145 °C at 20 °C/min, then at 8 °C/min to 200 °C and finally 4 °C/min to 320 °C, where it was held in isotherm for 20 min. H_2 gas with a pre-determined isotope composition was used as a monitoring gas, with H_3^+ factors measured daily. In order to assure consistency a squalene standard was co-injected with each sample. The average of this squalene δD was -152.8‰ with a standard deviation of 8.3. Samples were run in duplicate with the average of these runs presented in this paper.

Following the recommendation cited in Van der Meer et al. (2013) the δD_{alk} values were derived from combined C37:2 and C37:3 peaks due to fractionation differences between the two compounds.

d) Method adjustment

In an attempt to obtain more alkenones from the samples and clean up the alkenone fractions they were saponified to remove esters and potentially free additional alkenones by breaking up the macro molecular matrix. Additionally alkenone fractions were cleaned up by silver impregnated silica columns.

(i) Saponification

Saponification breaks ester-bonds between fatty acids and alcohols. Upon column chromatography using AlOx columns these polar molecules are retained on the stationary phase, eluting either in the polar fraction (alcohols) or remain on the column (fatty acids), and therefore effectively removing the esters from the ketone fraction. This process has no effect on the alkenones present in the sample leaving the ketone fractions relatively enriched in long chain alkenones. An additional benefit could be that the 3-D molecular matrix within each fraction breaks down thus freeing additional alkenones.

The saponification process involves reacting each sample with 1N potassium hydroxide (KOH)/H_2O in a reflux column at 130^{o}C for one hour. The pH of the solution was then decreased to ~pH 5 through addition of 2N hydrochloric acid/methanol (HCl/MeOH), in order to avoid fatty acid salt formation.

After saponification the organic fraction is cleaned by adding 2ml bi-distilled water and 2ml dichloromethane (DCM) and mixing vigorously. The water will dissolve any inorganic material as well as mix with the MeOH. This forms a H_2O/MeOH layer containing all the inorganics. The organic compounds will dissolve in the DCM rather than in the H_2O/MeOH layer. As the DCM is heavier and does not mix with the water/MeOH the mixture forms two layers, with the DCM layer underneath. This process therefore separates the inorganic material in the above layer and the organic compounds in the DCM layer below.

The DCM bottom layer is then pipetted out and the remaining layer of H_2O/MeOH can then be discarded. The DCM layer should then be passed through a Na_2SO_4 column in order to remove any water or MeOH that may have been inadvertently been taken by the pipette. The resulting extract is the new TLE which can be separated into fractions.

(ii) Silver nitrate impregnated silica

This step was performed on the ketone fraction as a clean up step, aiming to remove completely saturated compounds from the fraction. The ketone fraction is first dissolved in DCM and passed through a column containing Ag^+ silica as the stationary phase. The silver ions attract pi bonds present in the double bonds of molecules such as alkenones and fatty acids. Any molecule without a double bond (e.g. alkanes) will not be held in the stationary phase and therefore will elute with the DCM through the column resulting in the removal of any alkanes and other molecules that do not contain a double bond. Due to the presence of a C=C bond alkenones are held up in the stationary phase. These alkenones are then eluted with the more polar EtOAc:DCM (1:1, v:v) and collected in a pre-weighed vial. The third, most polar solvent (EtOAc) is then used to rinse out the sample ensuring that all alkenones have been detached from the stationary phase. Each column was wrapped in aluminium foil whilst eluting due to the susceptibility of Ag^+ silica to separate upon light exposure.

(iii) Other possible biomarkers

Due to the relatively low alkenone abundances (see results) across cores 1090b and 913b other biomarkers were also pursued that have been shown to be suitable for δD analysis.

1) Polar fraction analysis

Nelson & Sachs (2014) show that similarly to alkenones the δD of dinosterol and brassicasterol predominantly reflects the δD_w and salinity. These alcohols elute in the polar fraction. Due to their high polarities an additional step must be taken before the polar fractions can be injected into the GC - silylation.

In this step the polar fraction is reacted with 10µl N,O-Bis(trimethylsilyl)trifluoroacetamide (BSTFA), in the presence of pyridine (10µl), at 60°C. The subsequent reaction attaches a trimethlysilyl group (-$Si(CH_3)_3$) from the BSTFA to the alcohol group of the polar molecules thus reducing their polarity, and allowing them to be analysed by GC/GC-MS. The sterols within the polar fraction were identified using GC-MS. The GC-MS measurements were performed with an Agilent 7890B GC, coupled to an Agilent 5977 mass selective detector (MSD).

2) Apolar fraction analysis

The apolar fraction was also analysed for other potential biomarkers. A widespread biomarker is phytane derived from phytol, the esterifying sidechain of chlorophyll, and therefore originates from the vast majority of photosynthesising organisms (Yasser & Morsi, 2012). The widespread nature of this biomarker should lead to high abundances within the samples so long as organic compounds within the samples have evaded severe degradation/diagenesis through time. This high abundance should allow highly reliable δD measurements to be made allowing this δD record to be compared against the δD record of alkenones and sterols. In order to quantify the phytane present within the samples the apolar fraction was dissolved in hexane at 1mg/ml concentration before being injected in the GC.

e) Sea surface temperature proxies

Alkenones unsaturation ratios ($U_{37}^{K'}$)

The areas under the C37:2 & :3 alkenone peaks were calculated through manual integration of the mass 2 trace of the IR GC/MS from the same runs as the δD_{alk} were measured. This area was calculated on each sample on duplicate runs. The following calculations were performed separately on each run with only the result in Celsius being averaged across each sample, between duplicates, to give the approximate SST (°C).

$$U_{37}^{K'} = \frac{C37{:}\,2}{C37{:}\,3 + C37{:}\,2} \; (Brassell\ et\ al., 1986)$$

And subsequently,

$$SST\ (^{o}C) = \left(30.214 \cdot U_{37}^{K'}\right) - 1.725\ (\text{Müller et al.}, 1998)$$

Tetraether index (TEX_{86})

Tetraether index (TEX_{86}) analysis of glycerol dialkyl glycerol tetraethers (GDGTs) was performed on the polar fractions of samples from site 1090. Each polar fraction was re-dissolved in hexane/isopropanol (99:1, v:v) at a concentration of 2mg/ml. The solvent was then passed through a 0.4µm PTFE filter, removing any precipitates, before performing high performance liquid chromatography (HPLC) atmospheric pressure chemical ionization (APCI) mass spectrometry (MS), according to Schouten et al. (2007). The area under each GDGT peak was found through automatic integration using Agilent ChemStation software. From these areas the TEX_{86} value was calculated using the below equation.

$$TEX_{86} = \frac{GDGT\text{-}2 + GDGT\text{-}3 + GDGT\text{-}4'}{GDGT\text{-}1 + GDGT\text{-}2 + GDGT\text{-}3 + GDGT\text{-}4'}\ (Schouten\ et\ al. 2002)$$

Where: GDGTs 1 to 3 represent GDGTs with 1-3 cyclopentane moieties respectively. GDGT – 4' represents the regio-isomer of crenarcheol.

Subsequently from this TEX_{86} value the SST estimates could be made using the following equation.

$$SST\ (^{o}C) = (81.5 \cdot TEX_{86}) - 26.6\ (Kim\ et\ al. 2010)$$

f) Branched and isoprenoid tetraether (BIT) index

The same HPLC-MS analysis for TEX_{86} also provides the measurements required for the branched and isoprenoid tetraether (BIT) index, a proxy for terrestrial soil input (Hopmans et al., 2004). The following calculations were performed on the peak areas.

$$BIT = \frac{GDGT\text{-}I + GDGT\text{-}II + GDGT\text{-}III}{GDGT\text{-}I + GDGT\text{-}II + GDGT\text{-}III + GDGT\text{-}IV}\ (Hopmans\ et\ al. 2004)$$

Where: GDGTs I to III refer to the first three branched tetraethers with 4 to 6 branches respectively. GDGT – IV represents the regio-isomer of crenarcheol.

The resulting BIT value ranges from 0-1 with 0 indicating no terrestrial matter input and 1 indicating entirely terrestrial matter input.

3. Results & Discussion

i. Alkenone abundance

In total 70 samples across three cores from sites 913, 1090 and 925 were extracted and analysed for the presence of alkenones. Of this 70, alkenones were identified in 38 samples (10 from site 913, 4 from site 1090, and 14 from site 925). 10 of these samples (3 from 1090 and 7 from 925) contained alkenones in high enough abundance to measure δD_{alk}, offering a 7myr window across the EOT.

Clean up steps were taken as described in the materials and methods chapter, in an attempt to increase the alkenone yield and therefore provide more samples to be analysed. Figure 5 shows a typical result of the first clean up step, saponification, on a sample from site 1090.

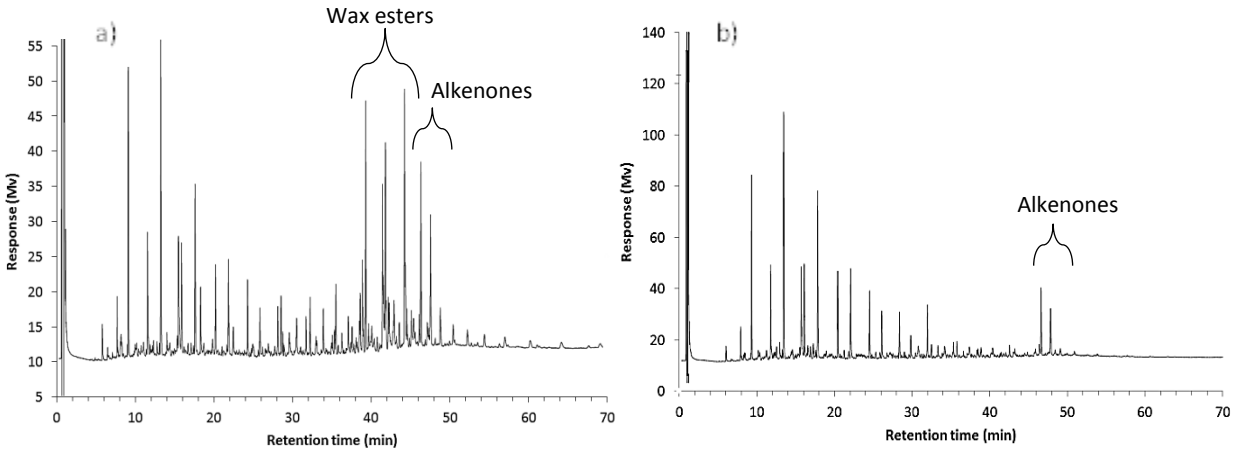

Figure 5. Saponification: GC outputs for ketone fraction of sample 1090, 29, 3. a) Shows the GC output resulting from the standard method. b) Shows the GC output following the saponification step. The peaks present at retention times relating to wax esters and alkenones are labelled.

This saponification step leads to a relative enrichment in alkenone yield, as well as a removal of wax esters that could co-elute with the alkenones and therefore cause uncertainties in δD_{alk} measurements.

The result of the clean up using an Ag^+ silica column is shown in figure 6 for one sample from site 913.

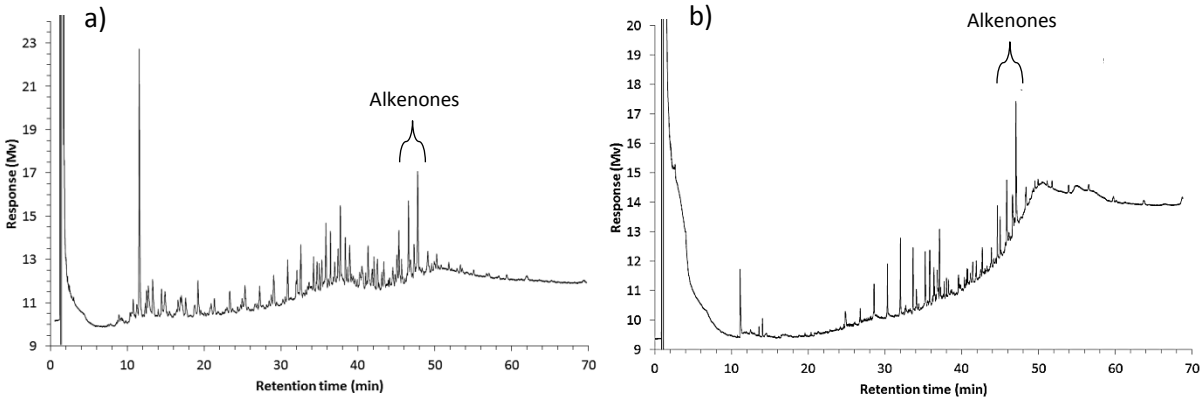

Figure 6. <u>Ag^+ silica column</u>: GC outputs for ketone fraction of sample 913, 29, 2. a) Shows the GC output resulting from the standard method. b) Shows the GC output following the use of an Ag+ silica column. The peaks present at the retention times related to the alkenones are labelled.

This clean up step can be seen to remove some of the non-alkenone compounds which elute prior to the alkenones, resulting in a relative enrichment in alkenone yield but also an enhancement of the background. The results seen in figures 5 & 6 are typical of the other samples cleaned through these steps. Neither clean-up step provides an absolute increase in alkenone yield, therefore the number of analysable samples remains the same.

The reasons for the low yield of alkenones within the samples analysed across the EOT are unclear but could be explained by the large scale oceanographic changes associated with the EOT. These changes would have greatly affected the surface ocean conditions, such as temperature and nutrient supply, leading to haptophyte distribution changes. Alkenones have been reported at 8 sites globally (Brassell et al., 2014) with $U_{37}^{K'}$ and $\delta^{13}C$ values being obtained from a number of them (Liu et al., 2008; Pagani et al., 2011), however few traverse the EOT in any great resolution (Figure 1 in Brassell et al., 2014). The low yields of this study suggest that alkenone abundances must have been minimal, even at these sites that report such occurrences.

The distribution of samples containing alkenones through time can be seen in figure 7, with further details of samples presented in table 1. Although neither core provides a complete traverse of the EOT, samples from site 1090 do cover both the EOT-1 and Oi-1 events (Pusz et al., 2011).

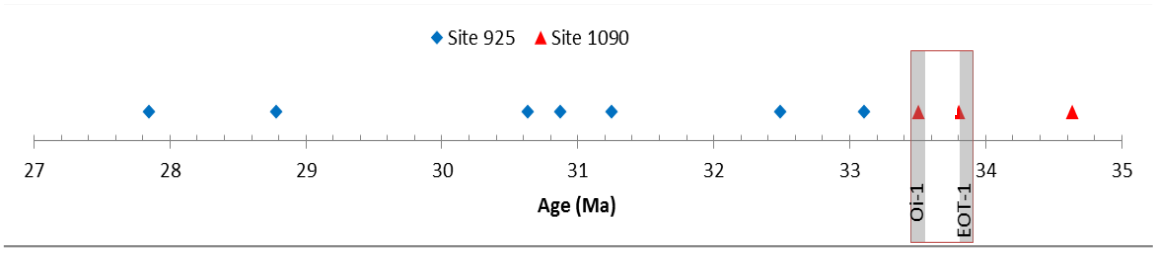

Figure 7. Alkenone occurrence: Distribution of alkenones used in this study against time from sites 1090 and 925. The EOT is shown with approximate EOT-1 and Oi-1 timings from the δ^{18}Ob record at site 1090 by Pusz et al. (2011) as shaded areas.

	Core	Section	Composite depth (m)	Age (ma)	δD_{alk} (‰)	$U^{K'}_{37}$ SST (°C)	TEX_{86} SST (°C)
Site 925	32	3	625.36	27.85	-165.2	26.4	--
	34H	3	644.68	28.78	-168.6	27.0	--
	40H	3	702.68	30.64	-184.0	25.5	--
	41	3	711.39	30.88	-171.6	24.9	--
	43H	3	724.95	31.25	-168.1	27.4	--
	48H	3	769.76	32.49	-157.9	24.8	--
	51	5	791.95	33.11	-149.1	27.5	--
Site 1090	25	5	240.67	33.51	-164.6	15.8	28.3
	26	5	252.62	33.80	-162.8	20.7	29.3
	29	3	278.02	34.64	-184.9	23.5	29.8

Table 1. Results overview: The samples from core analysed in this study which yield alkenones in high enough abundance to measure δD_{alk} along with their measured δD_{alk}, and SST values. TEX86 analysis only performed on samples from site 1090.

The apolar and polar fractions of a number of samples across the three cores were also analysed for the occurrence of other suitable biomarkers such as phytane and sterols, however none were found in the samples analysed and therefore these were not analysed on the IRMS.

ii. Results from ODP site 1090

At site 1090 δD_{alk} values shifted from -185‰ to -163‰ between 34.6 Ma and 33.8 Ma (figure 8). Thereafter the δD_{alk} remains relatively stable towards 33.5Ma, falling only slightly to -165‰. The $U^{K'}_{37}$ based temperature estimates for this core show a cooling between 34.6 Ma and 33.8 Ma from 23.5°C

to 20.7°C, and a larger subsequent cooling between 33.8 Ma and 33.5 Ma with temperatures falling from 20.7°C to 15.8°C. The temperature estimates from TEX_{86} also show a cooling, initially from 29.8°C to 29.3°C between 34.6 Ma and 33.8 Ma, which is followed by a cooling from 29.3°C to 28.3°C between 33.8Ma and 33.5Ma.

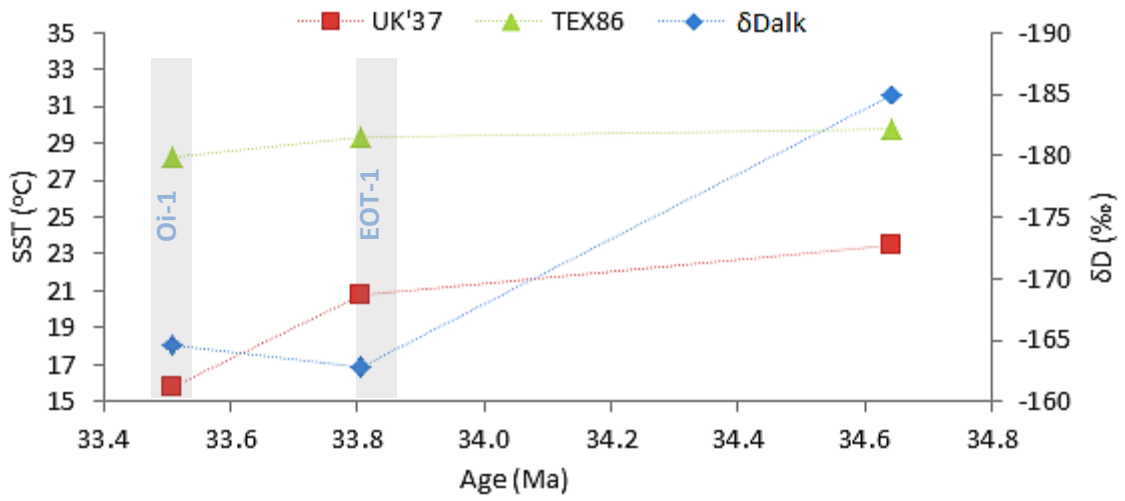

Figure 8. Site 1090: SST and δD_{alk} from the three alkenone bearing samples of ODP core 1090B prior to and through the EOT. The δD is flipped in line with the $\delta^{18}O$ convention to show warming as 'up' on the Y-axis. The approximate EOT-1 and Oi-1 timings at 33.8 and 33.5 respectively from the $\delta^{18}O_b$ record at site 1090 from Pusz et al. (2011) are shown as shaded areas.

The ~20‰ difference between δD_{alk} values at 34.6 and 33.8 Ma represents a positive δD_{alk} shift. This positive shift may be explained by the change in the isotopic composition of the water related to the glaciation of Antarctica at that time. Similarly the stabilisation in δD_{alk} thereafter may signify an absence of ice growth between 33.8 Ma and 33.5 Ma. The deuterium enriched sample at 33.8 Ma lies approximately on the EOT-1 oxygen isotope step (figure 8, shaded area), suggesting that the Antarctic glaciation occurred during this step, coinciding with this first oxygen isotope step. Furthermore the sample at 33.5 Ma is roughly situated on the Oi-1 step (figure 8, shaded area); therefore the relative stabilisation between these two later steps suggests that this second oxygen isotope step does not reflect an ice volume increase. Leaving the possibility of it being temperature related.

Although the absolute values between $U_{37}^{K'}$ and TEX_{86} SSTs are considerably offset from one another (by ~10°C), the temperature pattern displayed is much more similar. Temperatures from $U_{37}^{K'}$ and

TEX_{86} SST proxies both show only a relatively small decrease in the ~800kyr period between 34.6 Ma and 33.8 Ma of 2.8 ^{o}C and 1^{o}C respectively; whilst in the ~300kyr period between 33.8 Ma and 33.5 Ma the estimated cooling increases dramatically to 4.9 ^{o}C and 2 ^{o}C respectively. This pattern is significant as the lack of rapid cooling towards the EOT-1 step and its appearance instead at the Oi-1 step supports the suggestion seen in the δD_{alk} of an EOT-1 glaciation, without significant SST decrease, and an absence of substantial glaciation occurring at Oi-1 which instead displays a significant SST decrease.

It is important to note here that the temperature estimations presented above are of SSTs and therefore direct comparison to the oxygen isotope steps, which originates from benthic records, should be taken with care. SSTs respond much more rapidly to changes in atmospheric conditions than benthic temperatures however a lack of SST cooling during the δD_{alk} shift, and its appearance afterwards, is still significant.

The method used for $U_{37}^{K'}$ temperature reconstruction, utilising the output of an IRMS, fitted with a 25m column is not considered the optimum for this type of analysis, however the pattern of $U_{37}^{K'}$ temperatures presented here is in close agreement with those at the same site 1090 by Pagani et al. (2011) although with a near-constant offset (figure 9). Offsets of this magnitude (~2^{o}C) have been found to be common for samples measured at different laboratories (Rosell-Mele et al., 2001).

The BIT index analysis conducted at site 1090 showed an average value of 0.13 across the samples indicating very low terrestrial input over the site. The lack of terrestrial input verifies this site as open marine and therefore avoids the complications associated with near-shore settings on the δD_{alk} record (M'Boule et al., 2014; Kasper et al., 2015) and Tex86 SSTs (Weijers et al., 2006).

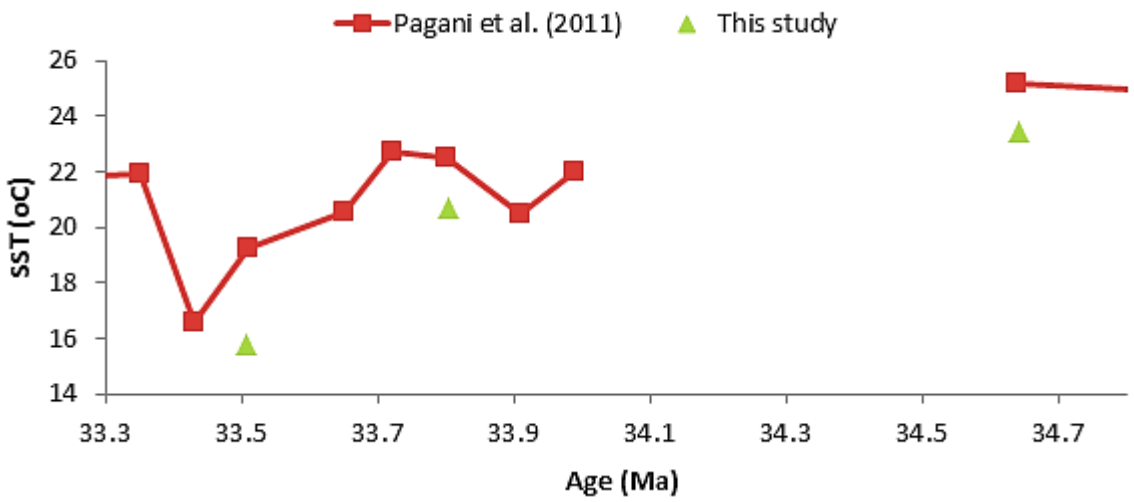

Figure 9. $U^{K'}_{37}$ site 1090: Two independent $U^{K'}_{37}$ SST records are shown; one from Pagani et al. (2011), and the other from this study.

iii. Results from ODP site 925

At site 925 (figure 10) δD_{alk} decreases gradually and almost linearly through the first four samples between 33.1 Ma and 30.9 Ma, from -149‰ to -172‰. After this, a steeper decline occurs towards 30.6 Ma, into a minimum across the record of -184‰. From this minimum at 30.6 Ma the δD_{alk} increases to -169‰ at 28.8 Ma and thereafter relatively stabilises towards an end value of -165‰ at 27.9 Ma.

The $U_{37}^{K'}$ SST estimates show a striking temperature dip across the first three samples. Between samples at 33.1 Ma and 32.5 Ma temperature decreases from 27.5°C to 24.8°C after which they recover back to 27.4 °C at 31.3 Ma. After this the temperature decreases once more to 24.9°C at 30.9 Ma before recovering gradually to 27.0 °C over the next two samples to 28.8 Ma. Thereafter the SST remains relatively stable, albeit with a slight decrease to 26.4°C at 27.9 Ma.

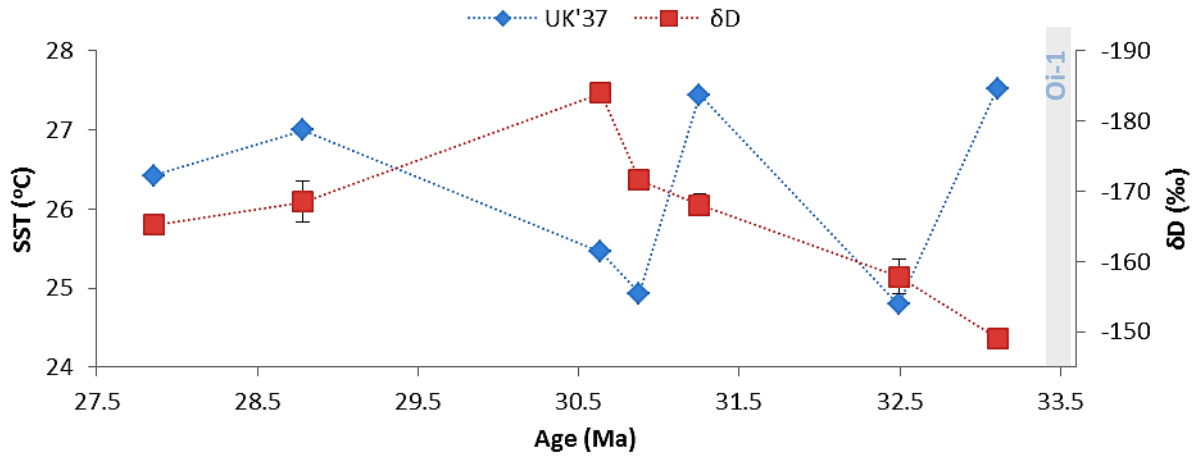

Figure 10. ODP site 925: SST and δD_{alk} from alkenone bearing samples of ODP core 925B directly following the EOT. The δD is flipped in line with the $\delta^{18}O$ convention to show warming as 'up' on the Y-axis. The approximate Oi-1 timing of 33.5 Ma from the $\delta^{18}Ob$ record at the South Atlantic site 1265 from Pusz et al. (2011) is shown as a shaded area.

The δD_{alk} record of site 925 which directly follows the EOT begins enriched in deuterium relative to the other samples. This first sample point at 33.1 Ma appears approximately 400kyr after the Oi-1 event at the end of the EOT. The δD enriched nature of this sample indicates δD enriched surface waters, which represents the surface ocean with a significantly glaciated Antarctic after the EOT. After this first sample point the δD_{alk} gradually decreases to the lowest δD_{alk} point at 30.6 Ma, possibly suggesting a slow thawing of the Antarctic ice. This rebound in the ice sheet is seen in other records such as $\delta^{18}O$, $\delta^{13}C$ and CCD (Coxall et al., 2005; Zachos & Klump, 2005) in which the original EOT change overshoots before returning towards pre-EOT values, albeit higher than before. Zachos et al. (2005) suggest that this overshoot is caused by negative feedbacks which are much more gradual than the positive feedbacks that lead to the transition.

Again the $U_{37}^{K'}$ record presented here was produced using an IRMS with a 25m column, and therefore these SST estimates should be taken as approximates. The $U_{37}^{K'}$ temperature record from site 925 seems at first to fluctuate wildly. However, with the exception of the sample at 32.5 Ma the SST record can be seen to be in an opposite phasing to that seen in the site 1090 records in which temperature decrease occurs with δD_{alk} decrease. The site 925 record shows enriched δD_{alk} coinciding with high SST. The exemption of the value at 32.5 Ma seems plausible as this would better fit the SST

reconstruction of Pagani et al. (2011) for this same site 925 (Figure 11). The decoupled nature of temperature and δD_{alk} at site 925 shows that counter intuitively increases in ice volume co-occur with increases in equatorial Atlantic SST, possibly indicating that localised processes affect δD_{alk} and SST separately, with a reduced signal of Antarctic ice volume and its associated climate changes.

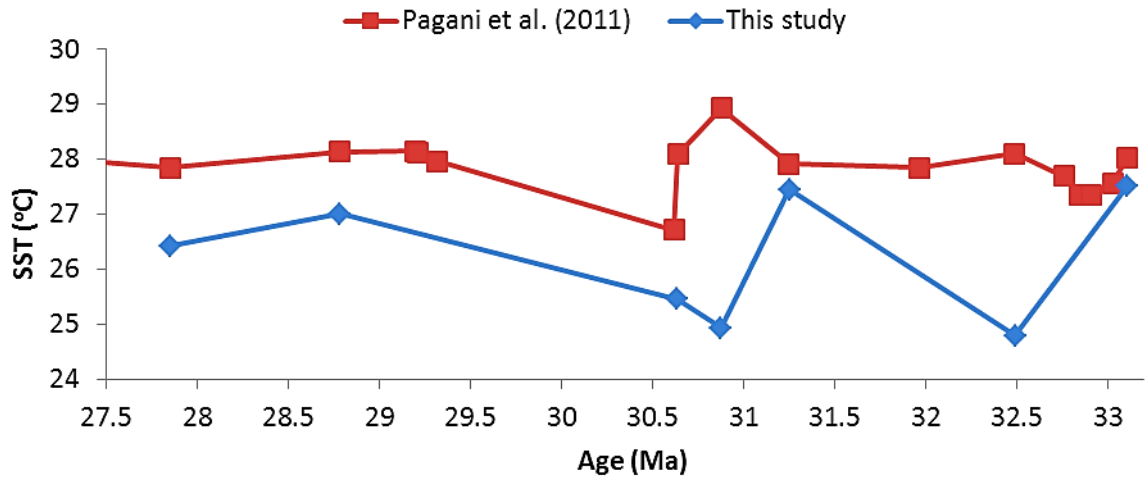

Figure 11. $U^{K'}_{37}$ site 925: Two independent $U^{K'}_{37}$ SST records are shown; one from Pagani et al. (2011), and the other from this study.

The SST estimates for the post-EOT begin at 27.5°C. Pagani et al. (2011) also find similar temperatures which remain largely unchanged through the EOT itself and then decrease in unison with the estimates presented here at approximately 31 Ma. The sudden decrease in SST significantly after the EOT could be caused by the widespread changes in ocean circulation and increases in upwelling that follow the EOT, as seen in many proxies (Coxall et al., 2005; Zachos & Klump, 2005; Via & Thomas, 2006; Livermore et al., 2007; Goldner et al., 2014). In light of this it would seem that the δD_{alk} at site 925 does nevertheless predominantly correspond to changes in ice volume whereas the changes in SST could be caused by circulation changes impacting local SST.

iv. DSDP site 511

Unpublished results from site 511 (figure 12) courtesy of van der Meer et al. offer both δD_{alk} and $\delta^{18}O$ of planktonic foraminifera ($\delta^{18}O_{pl}$) data across the EOT (figure 13). The δD_{alk} results can be seen to consist of two clusters of similar values, separated by

Figure 12. Site 511: map showing location of DSDP site 511

a ~400kyr gap. The first cluster consists of four samples, spanning from 34.21 Ma to 34.16 Ma. The first value of this cluster is -190‰, which is followed by a slight increase to two samples with values of -183% and -184‰, and a subsequent decline back to -188‰. The second cluster consists of seven samples spanning from 33.71 Ma to 33.64 Ma, starting with a value of -166‰ which remains almost unchanged for the next 2 samples before lowering to -173‰ at 33.68 Ma. Following this decrease the δD_{alk} then increases to -161‰ at 33.65 Ma, before decreasing once more towards a final value of -170‰ at 33.64 Ma.

The first point of the $\delta^{18}O_{pl}$ record occurring at 34.00 Ma measures 1.0‰. From this point the $\delta^{18}O$ decreases to 0.6‰ at 33.98, before increasing again over two samples back to 1.0‰ at 33.96Ma. Thereafter the record shows a decrease to 0.8‰ at 33.95 Ma, whereabouts it remains for the subsequent four samples before it decreases once more to 0.5‰ at 33.88 Ma. The next sample point appears at 33.70 Ma with a $\delta^{18}O$ value of 0.8‰, after which a seven-sample, near linear excursion concludes with a value of 2.1‰ at 33.68 Ma. After this the $\delta^{18}O$ recovers slightly to 1.8‰ at 33.66 Ma before stabilising at around 1.7‰.

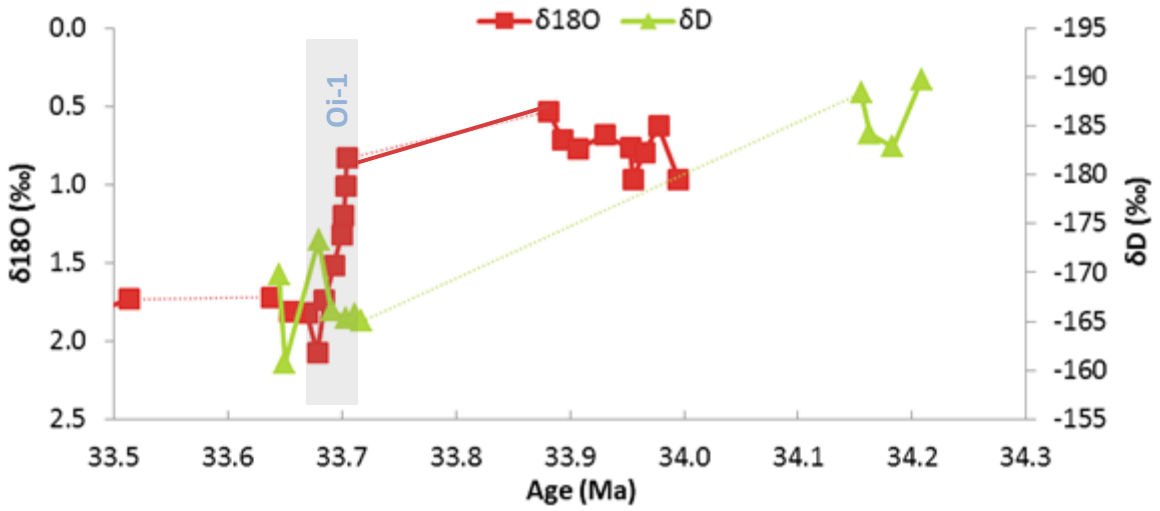

Figure 13. Site 511: δD_{alk} and $\delta^{18}O_{pl}$ records of samples from DSDP core 511 prior to and through the EOT. Site 511 results are courtesy of van der Meer et al. (unpublished). The δD and $\delta^{18}O$ is flipped in line with the $\delta^{18}O$ convention to show warming as 'up' on the Y-axis. Likely approximation of oxygen isotope step Oi-1 is shown in grey.

Between the two relatively stable δD_{alk} clusters a ~20‰ shift towards more deuterium rich values occurs, prior to 33.7 Ma. Again this shift may be explained through surface water deuterium enrichment caused by Antarctic glaciation. The $\delta^{18}O_{pl}$ record at site 511 shows a rapid 1.3‰ positive excursion, occurring in ~20kyr, at around 33.7 Ma. The magnitude of the $\delta^{18}O$ shift approximates the $\delta^{18}O$ shift seen at Oi-1 in other records (Coxall et al., 2005; Katz et al,. 2008; Pusz et al., 2011). Using dinoflagellates this $\delta^{18}O$ shift seen at 511 is confirmed as the Oi-1 event (Houben, 2012) The EOT-1 event is not recorded in this $\delta^{18}O_{pl}$ record, perhaps due to the apparent carbonate dissolution seen between 33.9 and 33.7 Ma.

The use of $\delta^{18}O_{pl}$ rather than $\delta^{18}O_b$ for this record, allows better comparison between δD_{alk} and $\delta^{18}O$ changes as both reflect surface waters. However this creates a problem when trying to relate the timing of the $\delta^{18}O_{pl}$ shift to an isotope step seen in $\delta^{18}O_b$ records globally. The different Oi-1 step timing seen at site 511 to those seen at site 1090 in other studies (Coxall et al., 2004; Katz et al., 2008; Miller et al., 2009; Puzs et al., 2011) could in part reflect this disparity between surface and abyssal waters. Having said this, even the timings of the steps seen between individual $\delta^{18}O_b$ records across many sites globally differ somewhat (Coxall et al., 2005; Miller et al., 2008; Miller et al., 2009; Houben et al., 2012).

However as both of these records reflect surface changes it can be concluded with a degree of certainty that the major ~20‰ positive δD_{alk} excursion, which could signify a major ice volume increase, must have occurred prior to the major $\delta^{18}O$ shift seen in the record. This is highly significant as it suggests that the $\delta^{18}O$ shift seen at the EOT may not be related to ice growth as previously thought.

Due to the co-varying nature of $\delta^{18}O_w$ and δD_w, any ice induced increase in δD_w must at least in part coincide with an oxygen isotope excursion (Craig & Gordon, 1965) and so it could be estimated that the δD_{alk} increase at site 511 coincides with this smaller oxygen isotope step, EOT-1. Only through a higher resolution record without significant carbonate dissolution could this estimation be verified.

v. Comparisons between sites

The two sites that provide δD_{alk} values across EOT, 1090 and 511, both show significant positive excursions in δD_{alk} (figure 14). These excursions are of the same ~20‰ magnitude, with similar pre- and post-EOT values (~-185‰ to ~-165‰) suggesting the same causal event. The similarities in the shifts at these sites, located on the other side of the ocean to one another also suggest that local salinity and hydrological changes, as well as biological factors such as growth rate do not significantly affect the δD_{alk}-δD_w signal in these records.

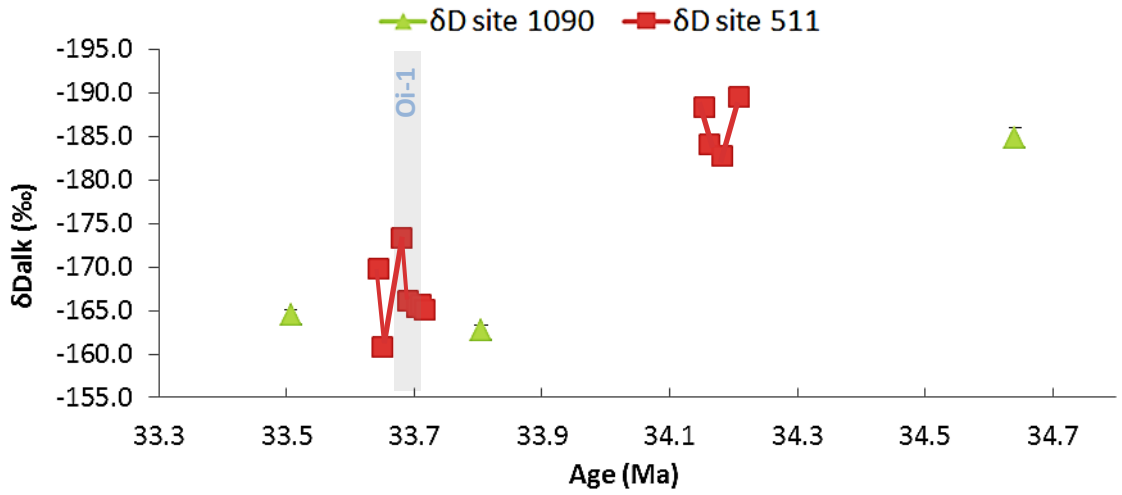

Figure 14. Sites 1090 and 913: The δD_{alk} records from site 1090 acquired in this study alongside that of site 511 (van der Meer, unpublished). The shaded grey area shows the estimated Oi-1 timing from site 511.

The proposition that both of these sites show the same causal event, unaffected by local oceanographic changes or biological factors, suggests that the ~20‰ δD_{alk} shift signifies a large widespread deuterium enrichment of surface water, as well as the associated increase in global salinity.

vi. Comparison of δD_{alk} to global $\delta^{18}O$

The global stacked benthic $\delta^{18}O$ record constructed by Zachos et al. (2001) compiles benthic $\delta^{18}O$ data from over 40 sites to provide a global scale picture of the deep ocean through time. Here the stacked record is compared to the data acquired in this study (figure 15).

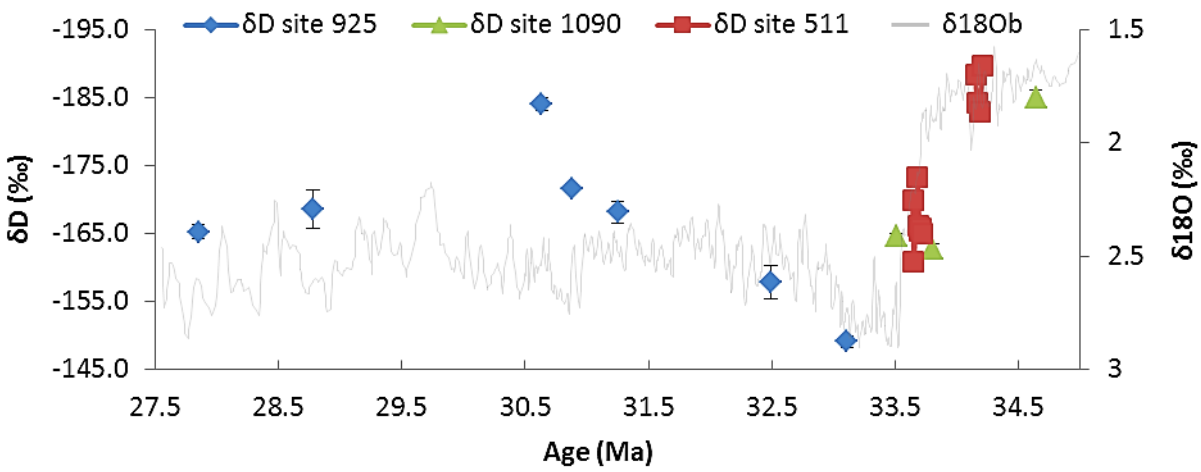

Figure 15. δD_{alk} against $\delta^{18}O_b$: The δD_{alk} at sites 925, 1090 and 511 against time, plotted with the stacked $\delta^{18}O_b$ record of Zachos et al. (2001). The δD and $\delta^{18}O$ axes are flipped in line with the $\delta^{18}O$ convention to show warming as 'up' on the Y-axis.

This data shows the δD_{alk} excursions at site 1090 occurring prior to the major $\delta^{18}O_b$ excursion associated with the EOT. It also displays the enriched δD_{alk} values of the equatorial site 925 immediately after the $\delta^{18}O_b$ excursion as compared to those at sites 511 and 1090, as well as its gradual reduction thereafter. It is also clear that between these two records there exists a ~15‰ offset.

It must be noted here that as the above $\delta^{18}O$ record in figure 15 is a global stack of benthic records this can only be taken as a global average and that at individual sites the magnitude of the excursion can differ remarkably. Also the use of this global stack conceals the two-step nature of this shift seen in many individual records (Coxall et al., 2025; Katz et al., 2008; Pusz et al., 2011).

Additionally, as already mentioned the δD_{alk} record produced reflects sea surface δD_w changes whilst the global stack reflects abyssal changes. It is possible that an extensive lag could exist between the changes in the surface δD_w and $\delta^{18}O_b$. This lag could then have concealed an abyssal temperature drop prior to the δD_w shift, which would suggest evidence for gateway opening. However this lag would have to be ~200-300kyr. This scale of lag time seems very unrealistic as on average the modern Thermohaline Circulation overturns deep water in 600 years (Toggweiler & Key, 2001).

Additionally the site 511 record with its planktonic oxygen isotope record showing the $\delta^{18}O$ shift occurring after the δD_w shift further eliminates the possibility of a significant lag.

In the modern ocean the δD_w values differ globally due to oceanic and atmospheric circulation patterns and Rayleigh distillation (Schmidt, 1999). This would also be true of the oceans in the Paleocene due to the intensified hydrological cycle (Carmichael et al., 2015). The intensified hydrological cycle would then increase the effect of Rayleigh distillation, leading to a strengthened latitudinal δD_w gradient. In order to better compare the two sites an adjustment for this gradient should be made. Schmidt et al. (1999) provide modern day $\delta^{18}O_w$ values for many sites globally which can be translated into δD_w through the meteoric water line (Craig, 1961). Table 2 shows this, as well as the difference between the present day δD_w of the tropical equatorial Atlantic and the temperate South Atlantic.

Location (site)	$\delta^{18}O_w$ (‰)	δD_w (‰)	δD_w difference (‰)
Equatorial Atlantic (site 925)	0.8	16.4	5.6
South Atlantic (sites 1090 & 511)	0.1	10.8	

Table 2. Latitudinal gradient: $\delta^{18}O_w$ values for modern site locations taken from Schmidt et al. (1999) converted into δD_w using meteoric water line of $\delta D_w = 8 * \delta^{18}O_w + 10$ ‰ (Craig, 1961), with the difference between converted δD_w values at the site locations.

This modern-day difference shown in table 2 can then be subtracted from the site 925 record allowing a better comparison between the south Atlantic (sites 1090 and 511) and equatorial Atlantic (site 925) across the EOT (figure 16).

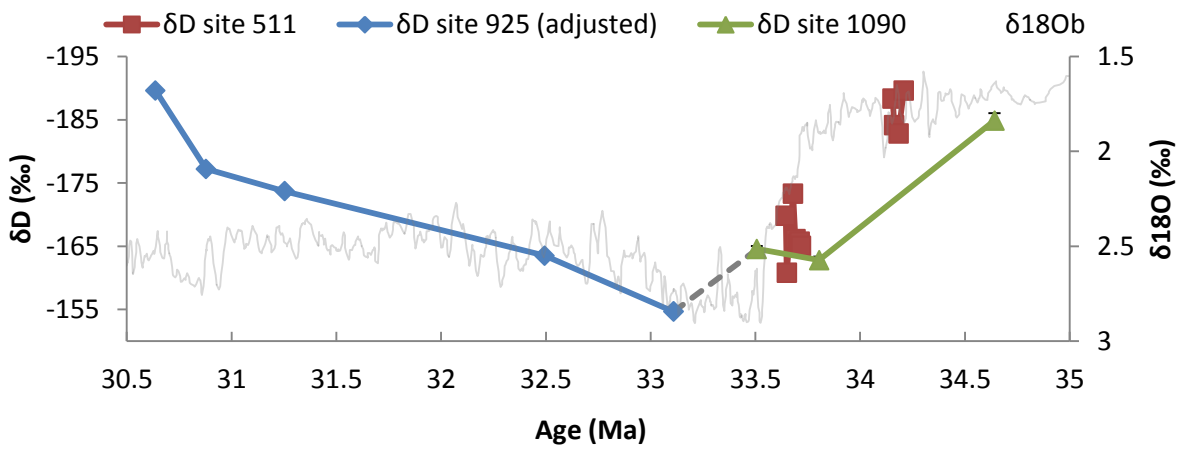

Figure 16. Site comparison: The adjusted δD_{alk} values for site 925 with the δD_{alk} values for sites 1090 and 511. Only the early section of site 925 immediately following the EOT is shown. These δD_{alk} values are also plotted with the global composite $\delta^{18}Ob$ from Zachos et al. (2001). Dashed grey line shows link between the equatorial and southern Atlantic sites, constructed through the latitudinal adjustment.

This adjustment shows only the difference caused by the δD_w gradient. In addition to this gradient there also exists a strong salinity gradient between the equatorial and south Atlantic as a result of differences in the evaporation vs. precipitation relationship. The result of this gradient is that the modern-day sea surface salinity of the equatorial Atlantic is as much as 2 practical salinity units (PSU) greater than the south Atlantic (Durack & Wijffels, 2010). As previously mentioned the salinity effect on fractionation during alkenone synthesis leads to an enrichment of δD_{alk} with increasing salinity. This salinity effect means that the adjustment shown above in figure 16 is an underestimation of the actual δD_{alk} difference between the sites. The full adjustment would better align the end δD_{alk} value of site 1090 with the earliest δD_w value of site 925, showing that the offset in the uncorrected values seen in figure 15 is related to latitude.

In addition to ice volume change the δD_w of surface water is affected by a number of other processes. Foremostly the hydrological cycle, in which water evaporates from the surface ocean at one location which then precipitates out at another. Due to Rayleigh fractionation this cycle results in the δD depletion and enrichment between regions that are net receivers of precipitation and those that are net sources of evaporation (Gat & Gonfiantini, 1981). Both the vigor of the hydrological cycle and the locations of these source and receiver regions change through time, mostly as the result of atmospheric and temperature changes (Hudson & Anderson, 1989). As a result the δD_w of surface

water also varies through time, independent of ice volume. This hydrological variance could therefore be the cause of the δD_{alk} shifts seen in the records presented above. However, this interpretation seems unlikely due to the close agreement of δD_{alk} values between the three sites, after adjustment. In the modern ocean hydrological processes at each core site differ, resulting in differences in δD_w (Gat & Gonfiantini, 1981). It is likely then that large scale hydrological changes that would be required to transmit a δD_w signal at the magnitude seen in these records would result in vastly differing δD_w values across the sites, which is not the case.

A second process that could result in a non ice-related δD_w shift is large scale ocean circulation change. Regions and depths of the ocean have different δD_w values (Schmidt et al., 1999). An influx of deuterium depleted water from one region/depth into the site due to a change in circulation direction, vigor or upwelling would cause a large δD_w shift, which would then be reflected in the δD_{alk}. This circulation change, occurring early in the EOT, could provide evidence for the gateway opening hypothesis as this hypothesis suggests large scale circulation changes occurred prior to glaciation. However again based on the agreement of the three sites, this circulation caused δD_w shift seems unlikely as it would have affected each site differently.

It can therefore be taken that the large, widespread increase in δD_w and salinity seen across the three cores presented in this thesis is most likely caused by an increase in continental ice volume. The proximity of sites 1090 and 511 to the Antarctic continent provides further assurance that the parallel δD_w shifts seen at these sites is related to ice growth. The lack of compelling evidence for northern hemisphere glaciation (Lear et al., 2008) suggests that this continental ice volume increase manifests itself in the glaciation of the Antarctic.

Through the meteoric water line (Craig, 1961); the 1‰ $\delta^{18}O$ shift across the entire EOT translates to a ~8‰ shift in δD_w. The 12‰ residue from the entire 20‰ shift δD_{alk} recorded at sites 1090 and 511 in this study must then be explained by salinity change. Using the relationship between the

fractionation factor of alkenone synthesis and salinity deduced by Schouten et al. (2006) this 12 ‰ δD_{alk} roughly corresponds to a 4 PSU increase.

4. Conclusions

This study set out to answer the research question; *at which $\delta^{18}O$ step of the EOT does the δD_{alk} excursion occur and how does this compare to temperature change?*

A significant 20‰ positive shift in δD_{alk} can be seen across the two records that traverse the EOT, sites 1090 and 511, and is alluded to in the record from site 925. This shift at least shows a co-occurrence with the changes related to the EOT. Unfortunately the lack of samples traversing the entire EOT containing abundant enough alkenones makes it difficult to answer the research question entirely. The very low sample resolution, 3 samples analysed, from Site 1090 makes it difficult to assess the precise timing of the δD_{alk} shift. However it is evident that the ~20‰ shift at site 1090 occurred at some point between 34.6 Ma and 33.8 Ma, certainly prior to Oi-1 and more in line with the EOT-1 event. Site 925 samples begin after the EOT, and therefore this data cannot be used to answer this research question. Analysis of site 511 again is impaired by a hiatus in samples containing enough alkenones throughout the EOT. However the $\delta^{18}O_{pl}$ record that was produced together with the δD_{alk} record offers the opportunity to define the Oi-1 step therefore interpret the δD_{alk} shift relative to this $\delta 18O_{pl}$ step. The δD_{alk} record of site 511 clearly suggests that a ~20‰ δD_{alk} shift occurred sometime between 34.1 Ma and 33.7 Ma, and similar to site 1090, prior to the Oi-1 event. The precise timing of the δD_{alk} shift is unknown, however since both the oxygen and hydrogen isotopic composition of seawater depends on ice volume it is expected that the hydrogen isotope shift co-occurs with a $\delta^{18}O$ shift and so seems likely that the δD_{alk} shift may have co-occurred with the EOT-1 event.

Although it has not been shown that the δD_{alk} shift coincided exactly with the EOT-1 $\delta^{18}O$ step, it is clear that the δD_{alk} shift occurred before the Oi-1 shift. This is significant in itself as it suggests that this major $\delta^{18}O$ step might not be related to ice volume, but possibly to temperature instead. The

further suggestion that the δD_{alk} increase is more likely to occur with the EOT-1 event therefore attributes this as ice volume related, rather than temperature. This is supported by the $U_{37}^{K'}$ SST estimates, finding that the significant 5^{o}C temperature decline across the EOT occurred after the δD_{alk}. These findings follow the glaciation first, followed by abyssal temperature trend. As has already been discussed, this trend offers support to the CO2 drawdown hypothesis, with AIS feedbacks, as the cause of the original glaciation of Antarctic occurring over the EOT.

These findings put atmospheric CO_2 right at the heart of this fundamental climate transition as a powerful climatic force, capable of determining the growth of a vast Antarctic Ice Sheet. It should not be taken lightly then that this same climatic force could also be capable of determining its future ablation.

5. References

Andersen, N., Paul, H. A., Bernasconi, S. M., McKenzie, J. A., Behrens, A., Schaeffer, P., & Albrecht, P. (2001). Large and rapid climate variability during the Messinian salinity crisis: evidence from deuterium concentrations of individual biomarkers. Geology, 29(9), 799-802.

Anderson, L. D., & Delaney, M. L. (2005). Middle Eocene to early Oligocene paleoceanography from Agulhas Ridge, Southern Ocean (Ocean Drilling Program Leg 177, Site 1090). Paleoceanography, 20(1).

Barker, P. F. (2001). Scotia Sea regional tectonic evolution: implications for mantle flow and palaeocirculation. Earth-Science Reviews, 55(1), 1-39.

Benthien, A., Andersen, N., Schulte, S., Müller, P. J., Schneider, R. R., & Wefer, G. (2002). Carbon isotopic composition of the C37: 2 alkenone in core top sediments of the South Atlantic Ocean: Effects of CO2and nutrient concentrations. Global biogeochemical cycles, 16(1), 12-1.

Berner, R. A. (2006). GEOCARBSULF: a combined model for Phanerozoic atmospheric O 2 and CO 2. Geochimica et Cosmochimica Acta, 70(23), 5653-5664.

Billups, K. & Schrag, D. P. (2003). Application of benthic foraminiferal Mg/Ca ratios to questions of Cenozoic climate change. Earth Planet. Sci. Lett. 209, 181–195.

Brassell, S. C. (2014). Climatic influences on the Paleogene evolution of alkenones. Paleoceanography, 29(3), 255-272.

Brassell, S. C., Eglinton, G., Marlowe, I. T., Pflaumann, U., & Sarnthein, M. (1986). Molecular stratigraphy: a new tool for climatic assessment. Nature, 320, 129-133

Carmichael, M., Lunt, D., & Pancost, R. (2015). Insights into the early Eocene hydrological cycle from an ensemble of atmosphere-ocean GCM simulations. In EGU General Assembly Conference Abstracts (Vol. 17, p. 8839).

Chaisson, W.P., & Pearson, P.N., 1997. Planktonic foraminifer biostratigraphy at Site 925: MiδDle Miocene–Pleistocene. In: Shackleton, N.J., Curry,W.B., Richter, C., Bralower, T.J. (Eds.), Proceeding of the Ocean Drilling Program: Scientific Results, 154, pp. 3–31.

Channell, J. E. T., Galeotti, S., Martin, E. E., Billups, K., Scher, H. D., & Stoner, J. S. (2003). Eocene to Miocene magnetostratigraphy, biostratigraphy, and chemostratigraphy at ODP Site 1090 (sub-Antarctic South Atlantic). Geological Society of America Bulletin, 115(5), 607-623.

Coxall, H. K., Wilson, P. A., Pälike, H., Lear, C. H., & Backman, J. (2005). Rapid stepwise onset of Antarctic glaciation and deeper calcite compensation in the Pacific Ocean. Nature, 433(7021), 53-57.

Craig, H. (1961). Isotopic variations in meteoric waters. Science, 133(3465), 1702-1703.

Craig, H., & Gordon, L. I. (1965). Deuterium and oxygen 18 variations in the ocean and the marine atmosphere.

DeConto, R. M., & Pollard, D. (2003). Rapid Cenozoic glaciation of Antarctica induced by declining atmospheric CO2. Nature, 421(6920), 245-249.

Diekmann, B., Kuhn, G., Gersonde, R., & Mackensen, A. (2004). Middle Eocene to early Miocene environmental changes in the sub-Antarctic Southern Ocean: evidence from biogenic and terrigenous depositional patterns at ODP Site 1090. Global and Planetary Change, 40(3), 295-313.

Diester-Haass, L., & Zahn, R. (1996). Eocene-Oligocene transition in the Southern Ocean: History of water mass circulation and biological productivity. Geology, 24(2), 163-166.

Durack, P. J., & Wijffels, S. E. (2010). Fifty-year trends in global ocean salinities and their relationship to broad-scale warming. Journal of Climate, 23(16), 4342-4362.

Eagles, G., & Jokat, W. (2014). Tectonic reconstructions for paleobathymetry in Drake Passage. Tectonophysics, 611, 28-50.

Ehrmann, W. (1998). Implications of late Eocene to early Miocene clay mineral assemblages in McMurdo Sound (Ross Sea, Antarctica) on paleoclimate and ice dynamics. Palaeogeography, Palaeoclimatology, Palaeoecology, 139(3), 213-231.

Ehrmann, W. U., & Mackensen, A. (1992). Sedimentological evidence for the formation of an East Antarctic ice sheet in Eocene/Oligocene time. Palaeogeography, Palaeoclimatology, Palaeoecology, 93(1), 85-112.

Ekart, D. D., Cerling, T. E., Montanez, I. P., & Tabor, N. J. (1999). A 400 million year carbon isotope record of pedogenic carbonate: implications for paleoatmospheric carbon dioxide. American Journal of Science, 299(10), 805-827.

Eldrett, J. S., Harding, I. C., Firth, J. V., & Roberts, A. P. (2004). Magnetostratigraphic calibration of Eocene–Oligocene dinoflagellate cyst biostratigraphy from the Norwegian–Greenland Sea. Marine Geology, 204(1), 91-127.

Francis, J. E., Marenssi, S., Levy, R., Hambrey, M., Thorn, V. C., Mohr, B., ... & DeConto, R. (2008). From greenhouse to icehouse–the Eocene/Oligocene in Antarctica. Developments in Earth and Environmental Sciences, 8, 309-368.

Gat, J. R., & Gonfiantini, R. (1981). Stable isotope hydrology. Deuterium and oxygen-18 in the water cycle.

Geletti, R., Lodolo, E., Schreider, A. A., & Polonia, A. (2005). Seismic structure and tectonics of the Shackleton fracture zone (Drake Passage, Scotia Sea). Marine Geophysical Researches, 26(1), 17-28.

Goldner, A., Herold, N., & Huber, M. (2014). Antarctic glaciation caused ocean circulation changes at the Eocene-Oligocene transition. Nature, 511(7511), 574-577.

Hemming, G. Hönisch, B. (2007). Chapter Seventeen Boron Isotopes in Marine Carbonate Sediments and the pH of the Ocean, In: Claude Hillaire–Marcel and Anne De Vernal, Editor(s), Developments in Marine Geology, Elsevier, 2007, Volume 1, Pages 717-734.

Herbert, T. D., Schuffert, J. D., Thomas, D., Lange, C., Weinheimer, A., Peleo-Alampay, A., & Herguera, J. C. (1998). Depth and seasonality of alkenone production along the California margin inferred from a core top transect. Paleoceanography, 13(3), 263-271.

Hill, D. J., Haywood, A. M., Valdes, P. J., Francis, J. E., Lunt, D. J., Wade, B. S., & Bowman, V. C. (2013). Paleogeographic controls on the onset of the Antarctic circumpolar current. Geophysical Research Letters, 40(19), 5199-5204.

Hogg, A. M. (2010). An Antarctic Circumpolar Current driven by surface buoyancy forcing. Geophysical Research Letters, 37(23).

Hönisch, B., & Hemming, N. G. (2005). Surface ocean pH response to variations in pCO2 through two full glacial cycles. Earth and Planetary Science Letters, 236, 305–314.

Hooker, J. J., Collinson, M. E., & Sille, N. P. (2004). Eocene–Oligocene mammalian faunal turnover in the Hampshire Basin, UK: calibration to the global time scale and the major cooling event. Journal of the Geological Society, 161(2), 161-172.

Hopmans, E. C., Schouten, S., Pancost, R. D., van der Meer, M. T., & Sinninghe Damsté, J. S. (2000). Analysis of intact tetraether lipids in archaeal cell material and sediments by high performance liquid chromatography/atmospheric pressure chemical ionization mass spectrometry. Rapid Communications in Mass Spectrometry, 14(7), 585-589.

Hopmans, E. C., Weijers, J. W., Schefuß, E., Herfort, L., Damsté, J. S. S., & Schouten, S. (2004). A novel proxy for terrestrial organic matter in sediments based on branched and isoprenoid tetraether lipids. Earth and Planetary Science Letters, 224(1), 107-116.

Houben, A. J. (2012) Triggers and consequences of glacial expansion across the Eocene-Oligocene Transition. Ph.D thesis, Utrecht University.

Houben, A. J., van Mourik, C. A., Montanari, A., Coccioni, R., & Brinkhuis, H. (2012). The Eocene–Oligocene transition: Changes in sea level, temperature or both?. Palaeogeography, Palaeoclimatology, Palaeoecology, 335, 75-83.

Huber, M., & Nof, D. (2006). The ocean circulation in the southern hemisphere and its climatic impacts in the Eocene. Palaeogeography, Palaeoclimatology, Palaeoecology, 231(1), 9-28.

Huber, M., Brinkhuis, H., Stickley, C. E., Döös, K., Sluijs, A., Warnaar, J., ... & Williams, G. L. (2004). Eocene circulation of the Southern Ocean: Was Antarctica kept warm by subtropical waters?. Paleoceanography, 19(4).

Hudson, J. D., & Anderson, T. F. (1989). Ocean temperatures and isotopic compositions through time. Transactions of the Royal Society of Edinburgh: Earth Sciences, 80(3-4), 183-192.

IPCC, 2013: Summary for Policymakers. In: Climate Change 2013: The Physical Science Basis. Contribution of Working Group I to the Fifth Assessment Report of the Intergovernmental Panel on Climate Change [Stocker, T.F., D. Qin, G.-K. Plattner, M. Tignor, S.K. Allen, J. Boschung, A. Nauels, Y. Xia, V. Bex and P.M. Midgley (eds.)]. Cambridge University Press, Cambridge, United Kingdom and New York, NY, USA

Ivany, L. C., Patterson, W. P., & Lohmann, K. C. (2000). Cooler winters as a possible cause of mass extinctions at the Eocene/Oligocene boundary. Nature, 407(6806), 887-890.

Ivany, L. C., Van Simaeys, S., Domack, E. W., & Samson, S. D. (2006). Evidence for an earliest Oligocene ice sheet on the Antarctic Peninsula. Geology, 34(5), 377-380.Katz et al. (2008

Kasper, S., van der Meer, M. T., Castañeda, I. S., Tjallingii, R., Brummer, G. J. A., Damsté, J. S. S., & Schouten, S. (2015). Testing the alkenone D/H ratio as a paleo indicator of sea surface salinity in a coastal ocean margin (Mozambique Channel). Organic Geochemistry, 78, 62-68.

Kasper, S., Van Der Meer, M., Mets, A., Zahn, R., Sinninghe Damsté, J. S., & Schouten, S. (2014). Salinity changes in the Agulhas leakage area recorded by stable hydrogen isotopes of C37 alkenones during Termination I and II. Climate of the Past, 10(1), 251-260.

Keller, G., MacLeod, N., & Barrera, E. (1992). Eocene–Oligocene faunal turnover in planktic foraminifera, and Antarctic glaciation. Eocene–Oligocene Climatic and Biotic Evolution. Princeton University Press, New Jersey, 218-244.

Kennett, J. P. (1977). Cenozoic evolution of Antarctic glaciation, the circum-Antarctic Ocean, and their impact on global paleoceanography. Journal of Geophysical Research, 82(27), 3843-3860.

Kim, J. H., Van der Meer, J., Schouten, S., Helmke, P., Willmott, V., Sangiorgi, F., ... & Damsté, J. S. S. (2010). New indices and calibrations derived from the distribution of crenarchaeal isoprenoid tetraether lipids: Implications for past sea surface temperature reconstructions. Geochimica et Cosmochimica Acta, 74(16), 4639-4654.

Kominz, M. A., Browning, J. V., Miller, K. G., Sugarman, P. J., Mizintseva, S., & Scotese, C. R. (2008). Late Cretaceous to Miocene sea-level estimates from the New Jersey and Delaware coastal plain coreholes: An error analysis. Basin Research, 20(2), 211-226.

Ladant, J. B., Donnadieu, Y., Lefebvre, V., & Dumas, C. (2014). The respective role of atmospheric carbon dioxide and orbital parameters on ice sheet evolution at the Eocene-Oligocene transition. Paleoceanography, 29(8), 810-823.

Lamy, F., Kaiser, J., Ninnemann, U., Hebbeln, D., Arz, H. W., & Stoner, J. (2004). Antarctic timing of surface water changes off Chile and Patagonian ice sheet response. Science, 304(5679), 1959-1962.

Lawver, L. A., & Gahagan, L. M. (1998). Opening of Drake Passage and its impact on Cenozoic ocean circulation. Oxford Monographs on Geology and Geophysics, 39, 212-226.

Lawver, L. A., Gahagan, L. M., & Campbell, D. A. (2003). Evolution of seaways in the circum-Antarctic region: impact on glaciation?. In EGS-AGU-EUG Joint Assembly (Vol. 1, p. 11361).

Lear, C. H., Bailey, T. R., Pearson, P. N., Coxall, H. K., & Rosenthal, Y. (2008). Cooling and ice growth across the Eocene-Oligocene transition. Geology, 36(3), 251-254.

Lear, C. H., Rosenthal, Y., & Slowey, N. (2002). Benthic foraminiferal Mg/Ca-paleothermometry: A revised core-top calibration. Geochimica et Cosmochimica Acta, 66(19), 3375-3387.

Lear, C. H., Rosenthal, Y., Coxall, H. K., & Wilson, P. A. (2004). Late Eocene to early Miocene ice sheet dynamics and the global carbon cycle. Paleoceanography, 19(4).

Liu, Z., Pagani, M., Zinniker, D., DeConto, R., Huber, M., Brinkhuis, H. & Pearson, A. (2009). Global cooling during the Eocene-Oligocene climate transition. Science, 323(5918), 1187-1190.

Livermore, R., Hillenbrand, C. D., Meredith, M., & Eagles, G. (2007). Drake Passage and Cenozoic climate: an open and shut case?. Geochemistry, Geophysics, Geosystems, 8(1).

Lodolo, E., & Tassone, A. (2010). Gateways and climate: the Drake Passage opening. Boll Geofis Teor Appl, 51, 77-88. Lyle et al. (2007)

M'boule, D., Chivall, D., Sinke-Schoen, D., Damsté, J. S. S., Schouten, S., & van der Meer, M. T. (2014). Salinity dependent hydrogen isotope fractionation in alkenones produced by coastal and open ocean haptophyte algae. Geochimica et Cosmochimica Acta, 130, 126-135.

Martos, Y. M., Maldonado, A., Lobo, F. J., Hernández-Molina, F. J., & Pérez, L. F. (2013). Tectonics and palaeoceanographic evolution recorded by contourite features in southern Drake Passage (Antarctica). Marine Geology, 343, 76-91.

Mawbey, E. M., & Lear, C. H. (2013). Carbon cycle feedbacks during the Oligocene-Miocene transient glaciation. Geology, 41(9), 963-966.

Miller, K. G., Wright, J. D., Katz, M. E., Browning, J. V., Cramer, B. S., Wade, B. S., & Mizintseva, S. F. (2008). A view of Antarctic ice-sheet evolution from sea-level and deep-sea isotope changes during the Late Cretaceous–Cenozoic. Antarctica: a keystone in a changing world, 55-70.

Miller, K. G., Wright, J. D., Katz, M. E., Wade, B. S., Browning, J. V., Cramer, B. S., & Rosenthal, Y. (2009). Climate threshold at the Eocene-Oligocene transition: Antarctic ice sheet influence on ocean circulation. Geological Society of America Special Papers, 452, 169-178.

Müller, P. J., Kirst, G., Ruhland, G., von Storch, I., & Rosell-Melé, A. (1998). Calibration of the alkenone paleotemperature index U 37 K' based on core-tops from the eastern South Atlantic and the global ocean (60 N-60 S). Geochimica et Cosmochimica Acta, 62(10), 1757-1772.

Nelson, D. B., & Sachs, J. P. (2014). The influence of salinity on D/H fractionation in dinosterol and brassicasterol from globally distributed saline and hypersaline lakes. Geochimica et Cosmochimica Acta, 133, 325-339.

Pagani, M. (2002). The alkenone-CO2 proxy and ancient atmospheric carbon dioxide. Philosophical Transactions of the Royal Society of London A: Mathematical, Physical and Engineering Sciences, 360(1793), 609-632.

Pagani, M., Huber, M., Liu, Z., Bohaty, S. M., Henderiks, J., Sijp, W., ... & DeConto, R. M. (2011). The role of carbon dioxide during the onset of Antarctic glaciation. Science, 334(6060), 1261-1264.

Pagani, M., Lemarchand, D., Spivack, A., & Gaillardet, J. (2005). A critical evaluation of the boron isotope-pH proxy: The accuracy of ancient ocean pH estimates. Geochimica et Cosmochimica Acta, 69(4), 953-961.

Pälike, H., Norris, R. D., Herrle, J. O., Wilson, P. A., Coxall, H. K., Lear, C. H., ... & Wade, B. S. (2006). The heartbeat of the Oligocene climate system. science, 314(5807), 1894-1898.

Pearson, P. N., & Chaisson, W. P. (1997). Late Paleocene to miδDle Miocene planktonic foraminifer biostratigraphy of the Ceara Rise. In Proceedings of the Ocean Drilling Program. Scientific results (Vol. 154, pp. 33-68). Ocean Drilling Program.

Pearson, P. N., Foster, G. L., & Wade, B. S. (2009). Atmospheric carbon dioxide through the Eocene–Oligocene climate transition. Nature, 461(7267), 1110-1113.

Pearson, P. N., McMillan, I. K., Wade, B. S., Jones, T. D., Coxall, H. K., Bown, P. R., & Lear, C. H. (2008). Extinction and environmental change across the Eocene-Oligocene boundary in Tanzania. Geology, 36(2), 179-182.

Pollard, D., & DeConto, R. M. (2005). Hysteresis in Cenozoic Antarctic ice-sheet variations. Global and Planetary Change, 45(1), 9-21.

Pusz, A. E., Thunell, R. C., & Miller, K. G. (2011). Deep water temperature, carbonate ion, and ice volume changes across the Eocene-Oligocene climate transition. Paleoceanography, 26(2).

Ravelo, A. C., & Hillaire-Marcel, C. (2007). Chapter Eighteen The Use of Oxygen and Carbon Isotopes of Foraminifera in Paleoceanography. Developments in Marine Geology, 1, 735-764.

Raymo, M. E. (1994). The initiation of Northern Hemisphere glaciation. Annual Review of Earth and Planetary Sciences, 22, 353-383.

Reguero, M. A., Marenssi, S. A., & Santillana, S. N. (2002). Antarctic Peninsula and South America (Patagonia) Paleogene terrestrial faunas and environments: biogeographic relationships. Palaeogeography, Palaeoclimatology, Palaeoecology, 179(3), 189-210.

Robert, C., & Kennett, J. P. (1997). Antarctic continental weathering changes during Eocene-Oligocene cryosphere expansion: Clay mineral and oxygen isotope evidence. Geology, 25(7), 587-590.

Rohling, E. J., & Cooke, S. (2003). Stable oxygen and carbon isotopes in foraminiferal carbonate shells. In Modern foraminifera (pp. 239-258). Springer Netherlands.

Rosell-Melé, A., Bard, E., Emeis, K. C., Grimalt, J. O., Müller, P., Schneider, R., ... & Wakeham, S. (2001). Precision of the current methods to measure the alkenone proxy UK37 and absolute alkenone abundance in sediments: Results of an interlaboratory comparison study, Geochem. Geophys. Geosyst., 2(7), 1046, doi: 10.1029/2000GC000141.

Sagnotti, L., Verosub, K. L., Roberts, A. P., Florindo, F., & Wilson, G. S. (2001). Environmental magnetic record of the Eocene-Oligocene transition in CRP-3 drillcore, Victoria Land Basin, Antarctica. Terra Antartica, 8, 507-516.

Scher, H. D., & Martin, E. E. (2006). Timing and climatic consequences of the opening of Drake Passage. Science, 312(5772), 428-430.

Scher, H. D., & Martin, E. E. (2008). Oligocene deep water export from the North Atlantic and the development of the Antarctic Circumpolar Current examined with neodymium isotopes. Paleoceanography, 23(1).

Schmidt, G. A. (1999). Forward modeling of carbonate proxy data from planktonic foraminifera using oxygen isotope tracers in a global ocean model. Paleoceanography, 14(4), 482-497.

Schmidt, G.A., G. R. Bigg and E. J. Rohling. 1999. "Global Seawater Oxygen-18 Database - v1.21" http://data.giss.nasa.gov/o18data/

Schouten, S., Hopmans, E. C., Schefuß, E., & Damste, J. S. S. (2002). Distributional variations in marine crenarchaeotal membrane lipids: a new tool for reconstructing ancient sea water temperatures?. Earth and Planetary Science Letters, 204(1), 265-274.

Schouten, S., Huguet, C., Hopmans, E. C., Kienhuis, M. V., & Sinninghe Damsté, J. S. (2007). Analytical methodology for TEX86 paleothermometry by high-performance liquid chromatography/atmospheric pressure chemical ionization-mass spectrometry. Analytical Chemistry, 79(7), 2940-2944.

Schouten, S., Ossebaar, J., Schreiber, K., Kienhuis, M. V. M., Langer, G., Benthien, A., & Bijma, J. (2006). The effect of temperature, salinity and growth rate on the stable hydrogen isotopic composition of long chain alkenones produced by Emiliania huxleyi and Gephyrocapsa oceanica. Biogeosciences, 3(1), 113-119.

Sessions, A. L., Burgoyne, T. W., Schimmelmann, A., & Hayes, J. M. (1999). Fractionation of hydrogen isotopes in lipid biosynthesis. Organic Geochemistry, 30(9), 1193-1200.

Shackleton, N. (1967). Oxygen isotope analyses and Pleistocene temperatures re-assessed.

Sijp, W. P., England, M. H., & Toggweiler, J. R. (2009). Effect of ocean gateway changes under greenhouse warmth. Journal of Climate, 22(24), 6639-6652.

Sijp, W. P., England, M. H., & Toggweiler, J. R. (2009). Effect of ocean gateway changes under greenhouse warmth. Journal of Climate, 22(24), 6639-6652.

Spero, H. J., Bijma, J., Lea, D. W., & Bemis, B. E. (1997). Effect of seawater carbonate concentration on foraminiferal carbon and oxygen isotopes. Nature, 390(6659), 497-500.

Stickley, C. E., Brinkhuis, H., Schellenberg, S. A., Sluijs, A., Röhl, U., Fuller, M., ... & Williams, G. L. (2004). Timing and nature of the deepening of the Tasmanian Gateway. Paleoceanography, 19(4).

Toggweiler, J. R., & Bjornsson, H. (2000). Drake Passage and palaeoclimate. Journal of Quaternary Science, 15(4), 319-328.

Toggweiler, J. R., & Key, R. M. (2001). Ocean circulation: Thermohaline circulation. Encyclopedia of Atmospheric Sciences, 4, 1549-1555.

Tripati, A. K., Eagle, R. A., Morton, A., Dowdeswell, J. A., Atkinson, K. L., Bahé, Y., ... & Thanabalasundaram, L. (2008). Evidence for glaciation in the Northern Hemisphere back to 44 Ma from ice-rafted debris in the Greenland Sea. Earth and Planetary Science Letters, 265(1), 112-122.

Urey, H. C. (1947). The thermodynamic properties of isotopic substances. Journal of the Chemical Society (Resumed), 562-581.

van der Meer, M. T., Benthien, A., Bijma, J., Schouten, S., & Damste, J. S. S. (2013). Alkenone distribution impacts the hydrogen isotopic composition of the C 37: 2 and C 37: 3 alkan-2-ones in Emiliania huxleyi. Geochimica et Cosmochimica Acta, 111, 162-166.

van der Meer, M. T., Benthien, A., French, K. L., Epping, E., Zondervan, I., Reichart, G. J., ... & Schouten, S. (2015). Large effect of irradiance on hydrogen isotope fractionation of alkenones in Emiliania huxleyi. Geochimica et Cosmochimica Acta, 160, 16-24.

Via, R. K., & Thomas, D. J. (2006). Evolution of Atlantic thermohaline circulation: Early Oligocene onset of deep-water production in the North Atlantic. Geology, 34(6), 441-444.

Wade, B. S., Houben, A. J., Quaijtaal, W., Schouten, S., Rosenthal, Y., Miller, K. G., ... & Brinkhuis, H. (2012). Multiproxy record of abrupt sea-surface cooling across the Eocene-Oligocene transition in the Gulf of Mexico. Geology, 40(2), 159-162

Weijers, J. W., Schouten, S., Spaargaren, O. C., & Damsté, J. S. S. (2006). Occurrence and distribution of tetraether membrane lipids in soils: implications for the use of the TEX 86 proxy and the BIT index. Organic Geochemistry, 37(12), 1680-1693.

Wolhowe, M. D., Prahl, F. G., Probert, I., & Maldonado, M. (2009). Growth phase dependent hydrogen isotopic fractionation in alkenone-producing haptophytes. Biogeosciences, 6(8), 1681-1694.

Yasser M. Moustafa and Rania E. Morsi (2012). Biomarkers, Chromatography and Its Applications, Dr. Sasikumar Dhanarasu (Ed.), ISBN: 978-953-51-0357-8, InTech

Zachos, J. C., & Kump, L. R. (2005). Carbon cycle feedbacks and the initiation of Antarctic glaciation in the earliest Oligocene. Global and Planetary Change, 47(1), 51-66.

Zachos, J. C., Breza, J. R., & Wise, S. W. (1992). Early Oligocene ice-sheet expansion on Antarctica: Stable isotope and sedimentological evidence from Kerguelen Plateau, southern Indian Ocean. Geology, 20(6), 569-573.

Zachos, J. C., Quinn, T. M., & Salamy, K. A. (1996). High-resolution (104 years) deep-sea foraminiferal stable isotope records of the Eocene-Oligocene climate transition. Paleoceanography, 11(3), 251-266.

Zachos, J., Pagani, M., Sloan, L., Thomas, E., & Billups, K. (2001). Trends, rhythms, and aberrations in global climate 65 Ma to present. Science,292(5517), 686-693.

Zhang, Y. G., Pagani, M., Liu, Z., Bohaty, S. M., & DeConto, R. (2013). A 40-million-year history of atmospheric CO2. Philosophical Transactions of the Royal Society A: Mathematical, Physical and Engineering Sciences, 371(2001), 20130096.